scientific reports

Check for updates

OPEN

Variable resolution machine learning optimization of antennas using global sensitivity analysis

Anna Pietrenko-Dabrowska[1] & Slawomir Koziel[1,2]✉

The significance of rigorous optimization techniques in antenna engineering has grown significantly in recent years. For many design tasks, parameter tuning must be conducted globally, presenting a challenge due to associated computational costs. The popular bio-inspired routines often necessitate thousands of merit function calls to converge, generating prohibitive expenses whenever the design process relies on electromagnetic (EM) simulation models. Surrogate-assisted methods offer acceleration, yet constructing reliable metamodels is hindered in higher-dimensional spaces and systems with highly nonlinear characteristics. This work suggests an innovative technique for global antenna optimization embedded within a machine-learning framework. It involves iteratively refined kriging surrogates and particle swarm optimization for generating infill points. The search process operates within a reduced-dimensionality region established through fast global sensitivity analysis. Domain confinement enables the creation of accurate behavioral models using limited training data, resulting in low CPU costs for optimization. Additional savings are realized by employing variable-resolution EM simulations, where low-fidelity models are utilized during the global search stage (including sensitivity analysis), and high-fidelity ones are reserved for final (gradient-based) tuning of antenna parameters. Comprehensive verification demonstrates the consistent performance of the proposed procedure, its superiority over benchmark techniques, and the relevance of the mechanisms embedded into the algorithm for enhancing search process reliability, design quality, and computational efficiency.

Keywords Antennas, EM-based design, Multi-resolution analysis, Global optimization, Sensitivity analysis, Surrogate modeling, Nature-inspired algorithms

Modern antenna design is an intricate task. The reasons are plenty: increasing requirements associated with emerging applications (5G[1,2], internet of things[3], microwave imaging[4], and many others[5–7]), the necessity to provide diverse operating capabilities (e.g., multi-band[8] and MIMO operation[9], polarization diversity[10,11], reconfigurability[12], beam steering[13]), the need for re-using the same hardware for different operating frequencies[14], as well as miniaturization trends[15]. The latter has become a particularly important consideration[16–19], fostering research on small antenna design[20–22]. Fulfilling stringent specifications leads to the development of geometrically sophisticated structures that involve auxiliary components (slots[23], stubs[24], transformers[25], shorting pins[26]), defected ground structures[27], metamaterials[28], substrate integrated waveguide cavities[29], or multi-layer implementations[30]. Topological complexity makes meticulous tuning of antenna parameters imperative; however, it must be realized using electromagnetic (EM) models (equivalent network representations[31,32] have little or no design utility), and simultaneously applied to all relevant parameters. Further, it might be subject to constraints, especially those related to physical size (e.g., antenna footprint)[33,34].

Engineering insight combined with parametric studies is still ubiquitous in parameter tuning of antenna structures[35,36]. Nevertheless, rigorous numerical algorithms are the only way to yield optimum designs. Despite the abundance of available methods, EM-based optimization is still challenging due to being CPU-heavy. Even local tuning typically requires dozens to hundreds of EM simulations. Global search is incomparably more expensive[37–39], particularly when using bio-inspired approaches[40–44]. On the other hand, global optimization is often needed. Examples include tasks featuring multiple local optima (array pattern enhancement[45,46], frequency selective surface or metasurface design[47,48]), design of compact antennas[49,50], unavailability of high-quality starting point (e.g., antenna geometry scaling over wide ranges of frequency[51]).

[1]Faculty of Electronics, Telecommunications and Informatics, Gdansk University of Technology, 80-233 Gdansk, Poland. [2]Engineering Optimization and Modeling Center, Reykjavik University, 101 Reykjavik, Iceland. ✉email: koziel@ru.is

These days, global optimization is predominantly realized using population-based bio-inspired techniques[52–61] that include genetic and evolutionary algorithms[62,63], evolutionary strategies[64], particle swarm optimizers (PSO)[65], differential evolution (DE)[66], and many others[67–75]. Arguably, the global search capability results from the exchange of data between the members of population[62], or mimicking hunting/preying habits[76] or social behaviour[66]. Unfortunately, nature-inspired methods are tremendously expensive with a few thousands of objective function evaluations on a lower end of typical computational budgets. Such costs are clearly prohibitive for direct EM-driven optimization unless parallelization is possible, contingent upon available resources[77]. Algorithmic speedup has been made possible by incorporating surrogate modeling techniques[78–82]. Practical frameworks are typically iterative procedures, with a fast metamodel (e.g., kriging, neural network, etc.[83–85]) constructed from accumulated EM simulation data and serving as a predictor to identify the optimum design location[86] (space exploitation), or to produce the infill points targeting the improvement of the model accuracy[87] (space exploration). These frameworks are often categorized as machine learning (ML) algorithms[88–91]. Despite potential advantages, difficulties in constructing reliable surrogate models, especially in higher-dimensional spaces and over wide ranges of design variables and frequencies, limit the range of applicability of the ML methods[92–94]. A possible workaround is performance-driven modelling techniques[95–98], incorporation of variable-fidelity EM models[99], or characteristic point methods[100–102]. The latter leverages reformulation of the problem regarding so-called feature points and close-to-linear dependence of their coordinates on the operating parameters[103]. However, this technique requires that the characteristic points exist over the complete design variable space.

This research introduces a low-cost technique for global antenna optimization, which follows the principles of machine learning. The underlying surrogate model and the core search engine are kriging interpolation and particle swarm optimizer, respectively. The infill criterion employs the merit function improvement according to the prediction of the underlying metamodel. The key acceleration factors encompass dimensionality reduction (realized through fast global sensitivity analysis, FGSA), and variable-resolution EM simulations. FGSA is developed to identify the parameter space directions that maximize antenna response variability. These vectors define the region of interest for the global search stage, executed using low-resolution EM analysis. Subsequent local parameter tuning involves a trust-region gradient based routine operating within the entire parameter space and carried out using high-fidelity EM analysis. Dimensionality reduction and the involvement of low-resolution models translate into superior performance and cost efficiency of our methodology. These have been corroborated by means of comprehensive verification experiments involving four planar antenna structures and several representative benchmark methods. The presented framework consistently yields designs of competitive quality, whereas its average CPU cost amounts to just 140 high-resolution EM analyses per run.

Variable-resolution machine learning for global antenna optimization using sensitivity-analysis-based dimensionality reduction

This section is devoted to providing the details of the suggested algorithmic framework. We commence by revisiting the formulation of the design task and offering essential background information on variable-resolution EM models (sections "EM-based antenna optimization" and "Variable-resolution computational models"). Subsequently, section "Low-cost global sensitivity analysis" overviews the fast global sensitivity analysis (FGSA), developed to delineate a dimensionality-reduced domain for the machine learning procedure, which is further discussed in section "Global search stage by machine learning". Additionally, section "Local tuning" delineates the local tuning algorithm, while section "Optimization framework summary" puts together the entire algorithm.

EM-based antenna optimization

Antenna optimization requires a rigorously defined merit function, which is assumed here to be scalar-valued. If several objectives are present, they are typically combined, e.g., using a weighted function approach[104] or transformed into constraints[105]. Using the notation and terminology gathered in Table 1, one may define the EM-driven optimization task as

$$\boldsymbol{x}^* = \arg \min_{\boldsymbol{x} \in X} U(\boldsymbol{x}) \qquad (1)$$

In (1), $\boldsymbol{x}^*$ represents the optimum design. Antenna responses, necessary to evaluate $U(\boldsymbol{x})$ are obtained with the help of full-wave EM simulation. Often, additional constraints are imposed upon (1), cf. the last two rows

Symbol	Meaning	Comments
$\boldsymbol{x} = [x_1 \ldots x_n]^T$	Designable parameters	Typically, antenna dimensions expressed in mm
$X = [\boldsymbol{l} \ \boldsymbol{u}]$	Parameter space	Parameter space is normally determined using lower and upper bounds on design parameters $\boldsymbol{l} = [l_1 \ldots l_n]^T$, and $\boldsymbol{u} = [u_1 \ldots u_n]^T$
$U(\boldsymbol{x})$	Objective (merit) function	The function U determines the design quality; it is defined so that better designs correspond to lower values of U
$g_k(\boldsymbol{x}) \leq 0, k = 1, \ldots, n_g$	Inequality constraints	Typically, constraints defined by imposing lower or upper acceptance thresholds for specific antenna responses over selected frequency ranges
$h_k(\boldsymbol{x}) = 0, k = 1, \ldots, n_h$	Equality constraints	Typically, constraints defined by imposing specific target values for selected operating figures (e.g., resonant frequency) of the antenna

Table 1. Parameter adjustment antennas: notation and terminology.

in Table 1. Their explicit handling, especially if g_k and/or h_k are expensive to evaluate, may be inconvenient. Often, a better option is implicit treatment using a penalty function approach[105]. According to this approach, the problem is reformulated as follows:

$$\mathbf{x}^* = \arg \min_{\mathbf{x}} U_P(\mathbf{x}) \tag{2}$$

where the objective function U_P is a linear combination of the merit function U and the penalty terms

$$U_P(\mathbf{x}) = U(\mathbf{x}) + \sum_{k=1}^{n_g+n_h} \beta_k c_k(\mathbf{x}) \tag{3}$$

Therein, the penalty functions $c_k(\boldsymbol{x})$, $k = 1, \ldots, n_g + n_h$, are defined to quantify constraint violations, whereas coefficients β_k control the contribution of particular penalty terms.

Representative antenna optimization tasks are listed in Table 2. The objective functions are formulated using the implicit approach should any constraints be present. The penalty functions therein (right-hand-side column) are defined to quantify relative constraint violation w.r.t. the given acceptance level (e.g., -10 dB for $|S_{11}|$). The frequency spectrum F depends on a particular problem: it may be either a discrete set of target frequencies $F = \{f_1 \ldots f_N\}$ for an N band antenna or a continuous interval(s), e.g., $F = [f_{1.1}\ f_{1.2}] \cup [f_{2.1}\ f_{2.2}] \cup \cdots \cup [f_{N.1}\ f_{N.2}]$, with N being a number of bands.

Variable-resolution computational models

Multi-fidelity computational models were applied to accelerate EM-driven procedures for over two decades[106,109–112]. In general, a reduction of the model fidelity can be achieved in diverse ways, for example, through the employment of simplified physics (e.g., equivalent networks in place of full-wave analysis), diminishing the computational domain, ignoring losses, assuming perfect electrical conductors[107], or reducing the structure's discretization density[108]. For antennas, the most universal approach is coarse-mesh EM simulation[107], which is also the only means for the majority of modern antennas. Low-fidelity modelling enables computational speedup while compromising the predictive power, cf. Fig. 1. The acceleration factor is very much dependent on the specific device and may vary from about two to as much as ten, given that the low-resolution EM analysis can render all relevant details of the system response.

We use two models, the low- and high-fidelity ones, $\boldsymbol{R}_c(\boldsymbol{x})$ and $\boldsymbol{R}_f(\boldsymbol{x})$, respectively. $\boldsymbol{R}_f(\boldsymbol{x})$ provides sufficient accuracy to ensure reasonable agreement between EM analysis predictions and the measurements of the antenna prototype. $\boldsymbol{R}_c(\boldsymbol{x})$ is used to conduct global sensitivity analysis, GSA (cf. section "Low-cost global sensitivity analysis"), and carry out global search (cf. section "Global search stage by machine learning"). The final optimization step, i.e., final tuning (cf. section "Local tuning") will be executed using $\boldsymbol{R}_f$. Because the two models are well-correlated, there is no need to incorporate any model correction at the GSA stage. Similarly, as the global search step yields an initial design for the final tuning, no low-resolution model correction is required here either. The above properties, directly following the modular architecture of the proposed design framework (cf. section "Optimization framework summary" for the flow diagram), make its implementation considerably simpler as compared to the algorithms relying on model alignment[109,113].
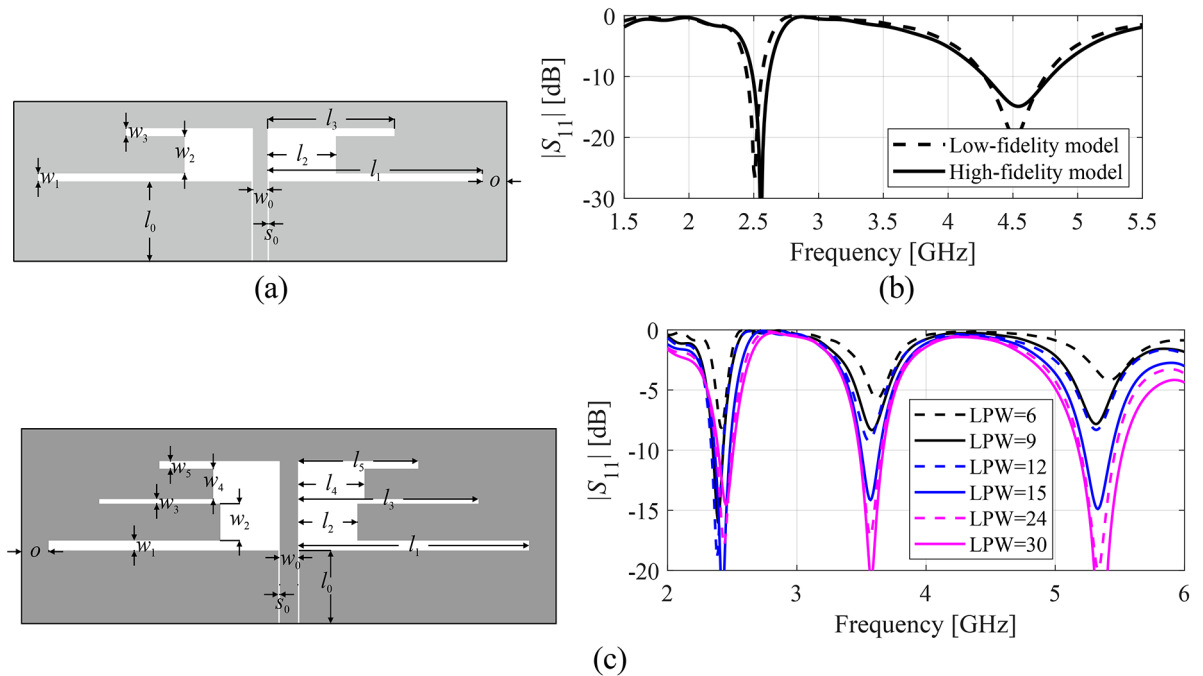
The selection of the low-fidelity model is carried out through visual inspection of antenna responses as illustrated in Fig. 1c. The mesh density (here, controlled using the lines-per-wavelength, LPW, parameter of CST Microwave Studio) gradually decreased until the response becomes heavily distorted and cannot adequately represent antenna characteristics. For the sample shown in Fig. 1c, this happens for LPW < 15.

Low-cost global sensitivity analysis

The design optimization framework proposed in this work is contingent upon behavioral models of antenna responses, utilized as predictors at the global search stage. The fundamental difficulty of behavioral modelling is the curse of dimensionality, further aggravated by the sheer size of the design variable space in terms of variable bounds and nonlinearity of antenna frequency characteristics. Dimensionality reduction is imperative to bring down the CPU expenses of surrogate model rendition while ensuring its sufficient accuracy. When it comes to global search procedures, the literature offers several approaches to identify parameters that can be potentially excluded from the search process. These may be categorized into variable screening (e.g., Pearson correlation coefficients[114], partial correlation coefficients[115], Morris method[116]), and global sensitivity analysis, GSA (e.g.,

Design scenario: verbal description	Objective function (1) and constraints	Objective function (3)
Design for best in-band matching within the frequency range F	$U(\boldsymbol{x}) = S(\boldsymbol{x}) = \max\{f \in F : |S_{11}(\boldsymbol{x},f)|\}$	$U_p(\boldsymbol{x}) = U(\boldsymbol{x})$
Design for maximum average in-band gain (in frequency range F); ensuring that in-band matching does not exceed -10 dB in F	$U(\mathbf{x}) = \overline{G}(\mathbf{x}) = \frac{1}{F}\int_F G(\mathbf{x}, f)df$ Constraint: $|S_{11}(\mathbf{x}, f)| \leq -10$ dB for $f \in F$	$U_P(\mathbf{x}) = \overline{G}(\mathbf{x}) + \beta_1 c_1(\mathbf{x})^2$ where $c_1(\mathbf{x}) = \left[\frac{\max(S(\mathbf{x})+10,0)}{10}\right]^2$

Table 2. Representative antenna optimization scenarios. Explanation of terms: f—frequency, $|S_{11}(\boldsymbol{x},f)|$—modulus of the reflection coefficient at design $\boldsymbol{x}$ and frequency f, $G(\boldsymbol{x},f)$—realized gain.

Fig. 1. Multi-resolution EM analysis: (**a**) a dual-band antenna; (**b**) $|S_{11}|$ obtained from the low- (- - -) and high-fidelity EM analysis (—). The high-resolution model simulates in 90 s, whereas the low-fidelity model requires just 25 s of the CPU time; (**c**) model selection: a triple-band antenna and EM models of various fidelities controlled by lines-per-wavelength (LPW) parameter of CST Microwave Studio. Visual inspection indicates that the models with LPW < 15 are heavily distorted and cannot adequately represent antenna characteristics.

Sobol indices[117], regression-based methods[118], or Jansen method[119]). Unfortunately, the mentioned techniques are generally expensive, i.e., require large numbers of data samples. At the same time, excluding individual variables is rarely an option in antenna design as the electrical and field properties are typically controlled through joint effects of several parameters. Consequently, it is recommended to develop a dimensionality reduction approach that satisfies the following conditions:

- It accounts for the entire parameter space;
- It can be carried out at low computational cost (e.g., less than a hundred of EM analyses);
- It does not focus on identifying individual parameters of high/low importance; instead, it allows for identifying essential parameter space directions that have major influence on antenna response variability.

Below, we provide the details of a fast global sensitivity analysis (FGSA) procedure developed having in mind the above-listed prerequisites.

Fast global sensitivity analysis (FGSA)
The main steps of FGSA include allocation of a set of randomly generated parameter vectors, setting up the relocation matrix **S**, and its spectral analysis leading to the eigenvectors e_j that represent the parameter space directions having a decreasing effects on the antenna response variability. The corresponding eigenvalues λ_j assess the importance of the particular vectors. By definition, e_j, $j=1, \ldots, n$, constitute an orthonormal basis in the decision variable space X. The operating steps of FGSA are as follows:

1. 1. Input parameters:

   - Parameter space X;
   - Computational model $R(x)$;
   - Number of samples N_s;

2. Generate N_s random vectors $x_s^{(k)} \in X$, $k=1, \ldots, N_s$, preferably in a uniform manner. Here, we use modified Latin Hypercube Sampling (LHS)[120];
3. Acquire EM simulation data $R(x_s^{(k)})$, $k=1, \ldots, N_s$;
4. For each $k=1, \ldots, N_s$, find $x_c^{(k)} = x_s^{(jmin)}$ such that

$$j_{\min} = \arg \min_{\substack{1 \leq j \leq N_s \\ j \neq k}} \left\| \mathbf{x}_s^{(k)} - \mathbf{x}_s^{(j)} \right\|$$

(4)

In other words, $\boldsymbol{x}_c^{(k)}$ is the vector closest to $\boldsymbol{x}_s^{(k)}$ in the norm sense;

5. Compute (normalized) relocation vectors

$$\mathbf{v}_s^{(k)} = \frac{\mathbf{x}_c^{(k)} - \mathbf{x}_s^{(k)}}{\left\|\mathbf{x}_c^{(k)} - \mathbf{x}_s^{(k)}\right\|} \tag{5}$$

and the corresponding (normalized) response variabilities

$$r_s^{(k)} = \frac{\left\|\mathbf{R}(\mathbf{x}_c^{(k)}) - \mathbf{R}(\mathbf{x}_s^{(k)})\right\|}{\left\|\mathbf{x}_c^{(k)} - \mathbf{x}_s^{(k)}\right\|} \tag{6}$$

for $k = 1, \ldots, N_s$;

6. Define a $N_s \times n$ relocation matrix $\boldsymbol{S}$ as

$$\mathbf{S} = \begin{bmatrix} r_s^{(1)}(\mathbf{v}_s^{(1)})^T \\ \vdots \\ r_s^{(N_s)}(\mathbf{v}_s^{(N_s)})^T \end{bmatrix} \tag{7}$$

The rows of $\boldsymbol{S}$ represent relocation vectors normalized with respect to their importance in terms of how they affect antenna response in the norm sense;

7. Perform spectral analysis of $\boldsymbol{S}$[121] in order to find its eigenvectors $\boldsymbol{e}_j$ (principal components) and the corresponding eigenvalues λ_j, $j = 1, \ldots, n$. The eigenvalues are ordered, so that $\lambda_1 \geq \lambda_2 \geq \ldots \lambda_n$.

It should be noted that the antenna response variability is computed for the pair of vectors $\boldsymbol{x}_s^{(k)}$ and their nearest neighbours $\boldsymbol{x}_c^{(k)}$, which is equivalent to computing (large-scale) directional derivatives. The latter determine the changes of frequency characteristics when moving from a given design $\boldsymbol{x}_s^{(k)}$ to $\boldsymbol{x}_c^{(k)}$. Because the number of such pairs is equal to N_s, the overall data gathered this way accounts for typical response sensitivity over the design variable space.

As explained in Step 7, the eigenvalues and eigenvectors are found through a spectral analysis (principal component analysis) of the $N_s \times n$ relocation matrix $\boldsymbol{S}$. It is carried out by singular value decomposition of the symmetric $n \times n$ covariance matrix $\boldsymbol{C} = \boldsymbol{S}_c^T \boldsymbol{S}_c / (N_c - 1)$, where $\boldsymbol{S}_c$ is the centered version of $\boldsymbol{S}$. We have $\boldsymbol{C} = \boldsymbol{U}\boldsymbol{\Sigma}\boldsymbol{V}^T$, where $\boldsymbol{U}$ is $n \times n$ unitary matrix, $\boldsymbol{\Sigma}$ is a diagonal matrix containing the eigenvalues, whereas columns of the $n \times n$ matrix $\boldsymbol{V}$ are the eigenvectors.

A subset of N_d vectors $\boldsymbol{e}_j$ corresponding to the largest eigenvalues will be used to determine a reduced-dimensionality region of the space X, denoted as X_d. The set X_d will serve as a domain for the global optimization step, as elaborated on in section "Global search stage by machine learning".

The number $N_d \in \{1, 2, \ldots, n\}$ is found as the smallest integer satisfying

$$\frac{\sqrt{\sum_{j=1}^{N_d} \lambda_j^2}}{\sqrt{\sum_{j=1}^{n} \lambda_j^2}} \geq C_{\min} \tag{8}$$

It should be emphasized that the left side of (8) represents an aggregated variability of antenna responses along the first N_d eigenvectors in relation to the total variability; $C_{\min}$ is a user-defined threshold, set to 0.9 in all verification experiments of section "Algorithm verification". Selecting N_d as in (8) with $C_{\min} = 0.9$ is equivalent to ensuring that the domain-defining directions account for at least ninety percent of the overall response variability.

It should be mentioned that the proposed dimensionality reduction approach may have some resemblance to projection-based model reduction methods such as principal component analysis (PCA) or proper orthogonal decomposition (POD)[134]. At the same time, our approach is focused on explicit identification of the directions responsible for antenna characteristic variability over specific (target) frequency ranges, whereas the computational model itself (here, EM analysis) is considered a black box. In particular, the model is not available in an analytical form and cannot be represented as a parameterized dynamical system. Consequently, techniques such as principal component analysis are not directly applicable to our case and unable to produce corresponding results. On the other hand, PCA is used here as one of the steps of FGSA, specifically spectral analysis of the relocation matrix $\boldsymbol{S}$. An example of another technique that employs PCA at the optimization stage

is[135], where the authors carry out spectral analysis on the set of designs ranked based on objective function value and obtain a reduced search space this way.

Dimensionality reduction: surrogate model domain
As mentioned earlier, the purpose of FGSA is to identify the most influential parameter space directions from the perspective of the system response variability. In particular, the majority of response changes are bounded to the sub-space spanned by the first N_d of these directions (N_d established according to (8)). This region, denoted as X_d, will be used as a domain for the global optimization step, and also serve as a surrogate's domain being the main component of the machine learning (ML) framework of section "Global search stage by machine learning". Formally, the set X_d is defined as

$$X_d = \left\{ \mathbf{x} \in X : \mathbf{x} = \mathbf{x}_c + \sum_{j=1}^{N_d} a_j \mathbf{e}_j \right\} \cap X \tag{9}$$

In other words, X_d is an intersection of the original variable space X and the affine sub-space.

$$\boldsymbol{x}_c + a_1 \boldsymbol{e}_1 + \ldots + a_{Nd} \boldsymbol{e}_{Nd} \tag{10}$$

where $\boldsymbol{x}_c = [\boldsymbol{l} + \boldsymbol{u}]/2$ (the centre of X), and a_j, $j = 1, \ldots, N_d$, are real numbers. Figure 2 provides a visualization of the set X_d. The main rationale behind dimensionality reduction is to facilitate the construction of the metamodel utilized as a predictor during the machine learning procedure. At the same time, as X_d accounts for the main changes of antenna responses, it provides sufficient flexibility in terms of global optimum identification.

Global search stage by machine learning

Within the framework proposed in this paper, the initial optimization step is global search conducted in the reduced domain X_d. Its role is to identify the region that encapsulates the optimum. The approximate solution found at this stage will be further refined through local tuning (cf. section "Local tuning"). Global search is realized using machine learning (ML). The ML process exploits a kriging interpolation surrogate and the PSO procedure as the core optimization engine. At this stage, we exclusively use the low-fidelity model $\boldsymbol{R}_c$.

The initial metamodel $\boldsymbol{s}^{(0)}(\boldsymbol{x})$ is utilized as a predictor upon launching the machine-learning-based global search algorithm. The assumed modelling technique is kriging interpolation[87]. The model domain is the reduced-dimensionality set X_d. The process of establishing $\boldsymbol{s}^{(0)}(\boldsymbol{x})$ involves generation of the training datasetm, which is carried out in two steps:

- $N_i N_d$ random samples $\boldsymbol{x}_B^{(k)}$, $k = 1, \ldots, N_i N_d$, are allocated uniformly in X_d, where N_i is the control parameter (here, we use $N_i = 20$); the temporary model $\boldsymbol{s}_{tmp}(\boldsymbol{x})$ is constructed using $\{\mathbf{x}_B^{(k)}, \mathbf{R}_c(\mathbf{x}_B^{(k)})\}_{k=1,\ldots,N_t N_d}$;
- The infill points are generated by identifying locations corresponding to the maximum mean square error (MSE) of the current surrogate as explained in (11) below.

Model refinement is continued until relative RMS does not exceed E_{max} (another control parameter of the proposed framework, here, set to twenty percent), or the total number of samples exceeds $2N_i N_d$ (maximum computational budget). Maximization of MSE enhances the global accuracy of the model within X_d. Upon termination, the most recent model $\boldsymbol{s}_{tmp}(\boldsymbol{x})$ becomes $\boldsymbol{s}^{(0)}(\boldsymbol{x})$, which is the first predictor employed in the global search process.

The operating steps of the initial surrogate model construction are as follows:

1. Input parameters:

   - Reduced-dimensionality domain X_d (cf. section "Dimensionality reduction: surrogate model domain");
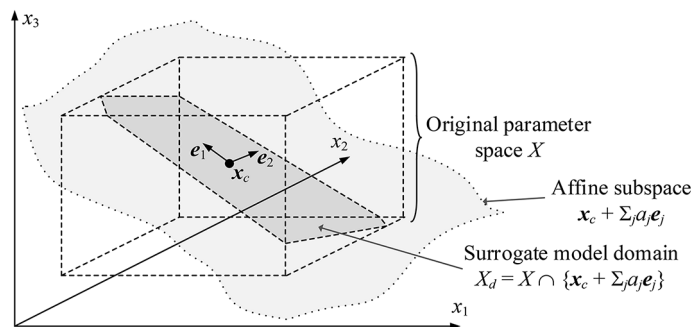
Fig. 2. Graphical illustration of the reduced-dimensionality domain X_d. Here, the original parameter space is three dimensional, whereas the set X_d is determined using two principal vectors $\boldsymbol{e}_1$ and $\boldsymbol{e}_2$. Note that X_d is an intersection of X and the affine subspace $\boldsymbol{x}_c + \Sigma_{j=1,2} a_j \boldsymbol{e}_j$.

6

- Modelling error threshold E_{max};
- Initial number of training samples N_iN_d (N_i is the user-defined parameter, N_d is the dimensionality of the reduced domain X_d).

2. Generate N_in samples $\boldsymbol{x}_B^{(k)} \in X_d$, $k = 1, \ldots, N_iN_d$, using uniform probability distribution;
3. Set $j = 0$;
4. Evaluate antenna responses $\boldsymbol{R}_c(\boldsymbol{x}_B^{(k)})$, $k = 1, \ldots, N_iN_d + j$, using EM simulation;
5. Construct surrogate model $\boldsymbol{s}_{tmp}(\boldsymbol{x})$ using dataset $\{\boldsymbol{x}_B^{(k)}, \boldsymbol{R}_c(\boldsymbol{x}_B^{(k)})\}_{k = 1, \ldots, NiNd + j}$;
6. Estimate model error E_{tmp} using K-fold cross-validation[122], $K = \min\{j, 10\}$;
7. **if** $E_{tmp} < E_{max}$ OR $j > 2N_iN_d$.

    Go to 12;
    end

8. Find an infill point by maximizing the mean square error (MSE) of the current

Surrogate model:

$$\mathbf{x}_B^{(N_iN_d+j)} = \arg \max_{\mathbf{x} \in X_d} MSE(\mathbf{s}_{tmp}(\mathbf{x})) \tag{11}$$

9. Set $j = j + 1$;
10. Evaluate antenna response $\boldsymbol{R}_c(\boldsymbol{x}_B^{(NiNd+j)})$ using EM simulation;
11. Go to 5;
12. Return $\boldsymbol{s}^{(0)}(\boldsymbol{x}) = \boldsymbol{s}_{tmp}(\boldsymbol{x})$;

Having defined $\boldsymbol{s}^{(0)}$, the machine learning (ML) algorithm is launched which iteratively refines the surrogate (using all available EM data), and employs it for producing subsequent approximations of the optimum design. The subsequent models are marked as $\boldsymbol{s}^{(j)}$, $j = 1, 2, \ldots$ The new candidate design $\mathbf{x}^{(i+1)}$, $i = 0, 1, 2, \ldots$, is determined by solving

$$\boldsymbol{x}^{(i+1)} = \arg \min_{\boldsymbol{x} \in X_d} U_s(\boldsymbol{x}, \boldsymbol{s}^{(i)}(\boldsymbol{x})) \tag{12}$$

The merit function U_S is analytically identical as the one defined in section "EM-based antenna optimization" but evaluated using $\boldsymbol{s}^{(i)}(\boldsymbol{x})$. This is indicated by the subscript S and explicit dependence of U_S on $\boldsymbol{s}^{(i)}$.

The underlying search algorithm utilized to solve (12) is the particle swarm optimizer (PSO)[123]. It should be emphasized that any nature-inspired procedure could be used at this stage: due to negligible evaluation cost of U_S, the computational budget can be set high, e.g., many thousands of objective function calls, which flattens out the differences between various search procedures (if any). PSO has been chosen due to being representative for this class of methods and widely popular.

From the ML perspective, the problem (12) establishes surrogate-predicted merit function enhancement to be an infill criterion[124]. The model $\boldsymbol{s}^{(i)}(\boldsymbol{x})$ is built based on all EM simulation data acquired until iteration i inclusive, i.e., $\{\mathbf{x}_B^{(k)}, \mathbf{R}(\mathbf{x}_B^{(k)})\}_{k=1,\ldots,2N_iN_d+i}$. Therein, $\mathbf{x}_B^{(2N_iN_d+i)} = \mathbf{x}^{(i)}$ for $i = 1, 2, \ldots$. The global search stage is considered accomplished if $||\mathbf{x}^{(i+1)} - \mathbf{x}^{(i)}|| < \varepsilon$ or the EM-evaluated objective function did not improve during $N_{no\_improve}$ most recent iterations. In the verification part of the work (section "Algorithm verification"), the following values of the mentioned parameters will be used: $\varepsilon = 10^{-2}$ and $N_{no\_improve} = 20$.

It should be noted that initial surrogate model construction and global search stage use different infill criteria, which is MSE maximization for initial model rendition, and objective function improvement for the global search stage. The rationale behind it is as follows. We aim at the initial surrogate model being as accurate as possible (therefore MSE is used as an infill criterion) so that global search. Having better model will expedite further optimization steps. Also, an acceptance threshold is introduced (E_{max}) achieving of which terminates the model construction process. Consequently, the used arrangement allows for a better control of the model accuracy. In the next stage, our only concern is identification of the region containing global optimum, therefore, objective function improvement as an infill criterion seems more appropriate keeping in mind computational efficiency (the process is fast anyhow due to initiating it with already good surrogate). Furthermore, the global search process is followed by local tuning, which allows for more precise optimum allocation. At the same time, it should be mentioned that many ML frameworks use different infill criteria, typically to ensure more balanced between exploration and exploitation (e.g., expected improvement)[124].

Local tuning

The ML-based global search is executed in the restricted domain X_d, which may prevent the process from identifying a truly optimum design. Therefore, a supplementary local tuning is employed, which is carried out over the entire parameter space X using accelerated gradient-based optimization. We use the trust-region (TR) routine[125] characterized in Fig. 3. The TR procedure employs a linear model of antenna outputs as a predictor, and

generates subsequent approximations of the optimum design by optimizing the predictor-based merit function over the search region of adaptively adjusted radius. When the algorithm is close to convergence, specifically, when $||x^{(i+1)} - x^{(i)}|| < 10\varepsilon_{TR}$, the sensitivity updating scheme is changed from full finite differentiation[126], to rank-one Broyden updating formula[127]. This reduces the number of EM simulations from $n+1$ to one per iteration. This substitution results in a notable enhancement of the computational efficiency. To ensure dependability, local tuning is executed using the high-fidelity model R_f.

Optimization framework summary

The proposed variable-resolution framework for global antenna optimization puts together the algorithmic mechanisms described in section "Low-cost global sensitivity analysis" through "Local tuning". Among these, the fast global sensitivity analysis (FGSA) and surrogate-assisted ML search are conducted using the low-fidelity

<u>Problem formulation</u>: Solve $x^* = \arg\min\{x \in X : U(x)\}$ (cf. (1)), with $x^{(0)}$ being an initial design;

<u>Algorithm operation</u>: Generate a series $x^{(i)}$, $i = 0, 1, …,$ of approximations to x^*. The new (candidate) vector $x^{(i+1)}$ is obtained by solving

$$x^{(i+1)} = \arg \min_{x; ||x-x^{(i)}|| \leq d^{(i)}} U_L(x, L^{(i)}(x)) \qquad (13)$$

where

$$L^{(i)}(x) = R_f(x^{(i)}) + J_R(x^{(i)}) \cdot (x - x^{(i)}) \qquad (14)$$

is a first-order Taylor expansion of R_f at $x^{(i)}$

<u>Objective function</u>: The function $U_L^{(i)}$ is analytically identical to U but evaluated using $L^{(i)}(x)$ rather than directly EM-simulated responses $R_f(x)$. This is by explicit dependence of U_L on $L^{(i)}(x)$.

<u>Gain ratio r</u>: EM-evaluated versus linear-model predicted objective function improvement

$$r = \frac{U(x^{(i+1)}) - U(x^{(i)})}{U_L(x^{(i+1)}) - U_L(x^{(i)})} \qquad (15)$$

<u>Trust region size $d^{(i)} > 0$</u>: Adaptively adjusted based on r; $d^{(i+1)} = d^{(i)}m_{incr}$ if $r > r_{incr}$, and $d^{(i+1)} = d^{(i)}/m_{decr}$ if $r < r_{decr}$; standard control parameter values are $r_{incr} = 0.75$, $r_{decr} = 0.25$, $m_{incr} = 1.5$, $m_{decr} = 2$ [125].

<u>Acceptance of the new iteration point</u>: $x^{(i+1)}$ is accepted only if $r > 0$ (i.e., EM-evaluated objective function has been improved); otherwise, the iteration is repeated with reduced TR size;

<u>Algorithm termination</u>: Convergence in argument ($||x^{(i+1)} - x^{(i)}|| < \varepsilon_{TR}$) or sufficient reduction of the TR size ($d^{(i)} \leq \varepsilon_{TR}$); the termination threshold is set to $\varepsilon_{TR} = 10^{-3}$

<u>Algorithm acceleration</u>: Jacobian matrix $J_R(x^{(i)})$ is estimated using finite differentiation (FD) [126] for the initial iterations of the optimization process, which incurs additional n EM analyzes of the antenna. When close to convergence (here, if $||x^{(i+1)} - x^{(i)}|| \leq 10\varepsilon_{TR}$), FD is replaced by a rank-one Broyden update [127], where the Jacobian matrix is updated using information about the design relocation and antenna response at the latest iteration [128]:

$$J_R^{(i+1)} = J_R^{(i)} + \frac{\left(f^{(i+1)} - J_R^{(i)} \cdot h^{(i+1)}\right) \cdot h^{(i+1)T}}{h^{(i+1)T} h^{(i+1)}}, \qquad i = 0, 1, … \qquad (16)$$

where $f^{(i+1)} = R_f(x^{(i+1)}) - R_f(x^{(i)})$, and $h^{(i+1)} = x^{(i+1)} - x^{(i)}$. This enables considerable computational savings as evaluation of (16) does not require any extra EM simulations.

Fig. 3. Accelerated trust-region (TR) search procedure employing a rank-one Broyden sensitivity updating formula[128].

EM model R_c (cf. section "Variable-resolution computational models"). Only the final (local) parameter tuning is realized using the high-resolution model R_f.

Table 3 enumerates the framework's control parameters. The last three parameters (ε, $N_{no\_improve}$, ε_{TR}) are related to the termination conditions, i.e., they only affect the optimization process precision. The remaining ones, N_r, N_i, and E_{max}, determine the reliability of the sensitivity analysis and intended accuracy of the metamodel. Consequently, their values are not critical because the number of random observables used by FGSA does not affect the outcome significantly. In contrast, N_i and E_{max} are only used to construct the initial metamodel, which is further enhanced during the ML process. Based on these comments, the proposed algorithm does not need to be specifically adjusted for a specific problem. This is illustrated by using an identical setup (cf. the last column of Table 3) for all numerical experiments of section "Algorithm verification".

Figure 4 illustrates the pseudocode of our optimization framework. The flow diagram is presented in Fig. 5. The majority of the search process, i.e., FGSA (Step 2), dimensionality-reduced domain definition (Step 3), construction of the initial surrogate (Step 4), as well as ML-based search (Steps 6 through 10), is performed using the low-fidelity model R_c. Only the final (gradient-based) parameter tuning is realized with the help of the high-fidelity model R_f to secure optimization process dependability.

Algorithm verification

We begin by illustrating the FGSA process in section "FGSA examples". The test cases are outlined in section "Verification antenna structures". For verification, our procedure is compared in section "Results" to several benchmark methods representing bio-inspired optimizers, machine learning, and conventional gradient-governed search. The latter is included to corroborate the presence of multiple local optima for the considered problems. Due to the stochastic nature of the algorithms, they are executed ten times each. The outcomes obtained this way are investigated in section "Discussion".

FGSA examples

Here, we consider two examples illustrating the FGSA procedure of section "Fast global sensitivity analysis (FGSA)". We start with a simple linear function $f(\boldsymbol{x}) = f([x_1 \ x_2]^T) = 3x_1 - 2x_2$, shown in Fig. 6. FGSA has been executed using twenty random samples. The first eigenvector $\boldsymbol{e}_1 = [0.84 -0.53]^T$, which agrees with the normalized gradient of $f(\boldsymbol{x})$, $\boldsymbol{g} = [0.83 -0.55]^T$ (the latter determines the direction of maximum variability owing to linearity of f). Figure 7 shows another example, where the function f is defined to allow visual assessment of the maximum variability (the vector perpendicular to the 'ripples'). Again, this observation agrees with the results obtained using FGSA.

Verification antenna structures

The geometries of test antennas have been shown in Fig. 8. Table 4 contains the essential data on all structures (substrate parameters, design variables, target frequencies, parameter ranges, etc.). The devices are named Antenna I, II, III, and IV, respectively. The EM models are prepared and evaluated in CST Microwave Studio. The time-domain solver is utilized for simulation purposes[133]. The low-resolution models R_c are set up by restricting the mesh density of the respective devices so that the simulated response still properly represents the critical features of the antenna, such as resonances. The high-resolution model R_f is determined using the grid convergence study with the discretization set to the level increasing of which does not have visible effects on frequency characteristics. The grid convergence study is understood as gradual increase of the mesh density and visual inspection of the antenna characteristics produced by EM simulation. The high-fidelity model is set up at the mesh density for which its further refinement does not alter the antenna responses in a noticeable manner. The time evaluation ratio between R_f and R_c is 3.7, 2.3, 8.3, and 3.8 for Antenna I through IV. Clearly, higher ratio will lead to higher computational savings.

All verification problems are intrinsic because of large parameter spaces (dimensionality from six to fourteen, the mean value of the ratio between the upper and lower bound reaching 4.2, 8.4, 2.8, and 2.6 for Antennas I through IV) as well as considerable nonlinearity of antenna characteristics, both with respect to frequency and design variables.

Parameter	Meaning	Default value
N_r	Number of random observables for fast global sensitivity analysis (FGSA), cf. section "Low-cost global sensitivity analysis"	50
N_i	Multiplier for the number of uniformly-distributed data samples for initial surrogate model construction; the actual number of samples is $N_i N_d$, with N_d being the dimensionality of the reduced domain X_d (cf. section "Global search stage by machine learning")	20
E_{max}	Maximum value of relative RMS error of the initial surrogate model (error estimated using cross-validation), cf. section "Global search stage by machine learning"	20%
ε	Termination threshold for convergence in argument, cf. section "Global search stage by machine learning"	10^{-2}
$N_{no\_improve}$	Termination threshold for no objective function value improvement, cf. section "Global search stage by machine learning"	10
ε_{TR}	Termination threshold for local parameter tuning stage, cf. section "Local tuning"	10^{-3}

Table 3. Control parameters of the proposed variable-resolution global optimization algorithm.

1. Input parameters:
   - Definition of the objective function U (cf. Section 2.1);
   - Assignment of the low- and high-resolution antenna models, $\boldsymbol{R}_c$ and $\boldsymbol{R}_f$, respectively;
   - Design space X (interval $[\boldsymbol{l} \; \boldsymbol{u}]$, where $\boldsymbol{l}$ and $\boldsymbol{u}$ are lower and upper bounds for designable parameters);
   - Control parameters (N_r, N_i, E_{max}, termination thresholds ε and $N_{no\_improve}$, cf. Table 1);

2. Generate N_r random observables at low-resolution level, and perform the FGSA procedure (cf. Section 2.3) to determine surrogate model domain dimensionality N_d and the spanning vectors $\boldsymbol{e}_k$;

3. Define dimensionality-reduced surrogate model domain X_d (cf. Section 2.3.3);

4. Construct initial surrogate model $\boldsymbol{s}^{(0)}(\boldsymbol{x})$ using sampled low-resolution model data, cf. Section 2.4.1 (also, | 8);

5. Set $i = 0$;

6. Obtain infill point $\boldsymbol{x}^{(i+1)}$ by solving (12) using the PSO algorithm:

$$\boldsymbol{x}^{(i+1)} = \arg \min_{\boldsymbol{x} \in X_d} U_S(\boldsymbol{x}, \boldsymbol{s}^{(i)}(\boldsymbol{x}))$$

7. Update the dataset: $\{\boldsymbol{x}_B^{(k)}, \boldsymbol{R}_c(\boldsymbol{x}_B^{(k)})\}_{k=1, \ldots, 2N_iN_d + i}$, where $\boldsymbol{x}_B^{(2N_iN_d+i)} = \boldsymbol{x}^{(i)}$ for $i = 1, 2, \ldots$.

8. Set $i = i + 1$;

9. Construct the surrogate model $\boldsymbol{s}^{(i)}(\boldsymbol{x})$ using the updated low-resolution dataset;

10. **if** $\|\boldsymbol{x}^{(i)} - \boldsymbol{x}^{(i-1)}\| < \varepsilon$ OR no objective function improvement for $N_{no\_improve}$ iterations
    Go to 11;
    end

11. Go to 6;

12. Perform local tuning over the original parameter space X, cf. Section 2.5

$$\boldsymbol{x}^* = \arg \min_{\boldsymbol{x} \in X} U(\boldsymbol{x})$$

The starting point is vector $\boldsymbol{x}^{(i)}$ found during the global search stage;

13. Return $\boldsymbol{x}^*$;

Fig. 4. Pseudocode of the variable-resolution machine-learning search procedure. The essential part of the algorithm is dimensionality-reduced surrogate whose domain is established using the proposed fast global sensitivity analysis scheme.

Results

Antennas I through IV were optimized using the algorithm of section "Variable-resolution machine learning for global antenna optimization using sensitivity-analysis-based dimensionality reduction", and several comparison methods listed in Table 5. For all antenna structures, the proposed procedure is executed using identical control parameter setup as elaborated on in Table 3. The benchmark set includes four algorithms:

- Algorithm I: particle swarm optimizer (PSO)[123], employed as a flagship bio-inspired method. It is executed with the budget of 500 (Version I) and 1000 (Version II) objective function calls. These numbers are low for population-based methods; however, the algorithm running time (two to three days) is considerable due to repetitive EM simulations.
- Algorithm II: differential evolution utilizes as one of the most popular state-of-the-art population based algorithms[136]. The algorithm is excuted using 1000 function calls as a computational budget.
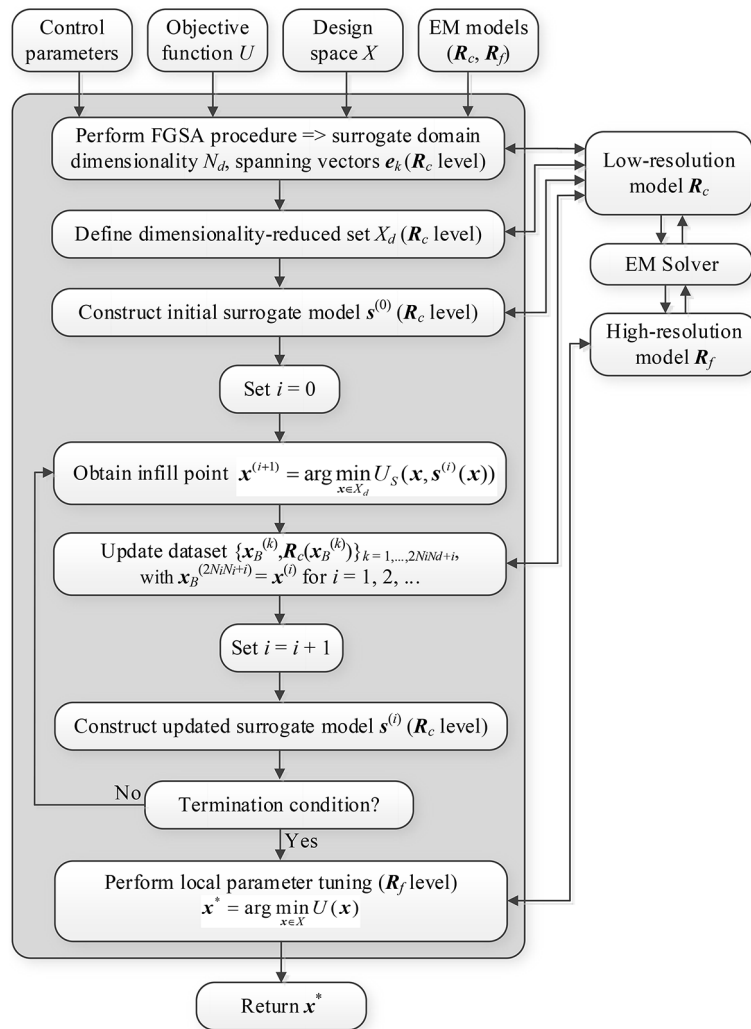
Fig. 5. Flow diagram of the variable-resolution machine-learning procedure for global antenna optimization.

- Algorithm III: Grey Wolf optimization[37], one of the recent and popular bio-inspired algorithms. Again, the computational budget is set to 1000 EM simulations.
- Algorithm IV: multiple-start gradient search, utilized to corroborate multimodality of the considered optimization tasks. In this study, it is conducted by means of the TR algorithm similar to the one explained in Fig. 4.
- Algorithm V: a machine-learning procedure working with kriging surrogates and the same mechanism for generating the infill points as the proposed technique. The major difference is that the algorithm operates within the original design space X. This technique is considered to demonstrate the advantages of dimensionality reduction.
- Algorithm VI: a machine-learning routine working along the lines of what was considered in section "Variable-resolution machine learning for global antenna optimization using sensitivity-analysis-based dimensionality reduction" but exclusively using the R_f model. We include this method to quantify the advantages of employing variable-resolution EM simulations.

Tables 6, 7, 8, 9 contain the results for all test antennas. Due to the presence of random components within the algorithms, they were executed ten times each. The reported data include the cost function value and the CPU cost entailed by the search process, both averaged over all algorithm runs. Additionally, the tables provide information about the number of runs for which a given procedure was able to produce design whose actual operating frequencies match the assumed targets. The success rate can be considered a measure of the reliability and solution repeatability of the search process.

Finally, Figs. 9, 10, 11, and 12 illustrate antenna characteristics for the designs produced during the selected executions of the suggested methodology. Shown are responses upon concluding the global search stage, and at the final designs.
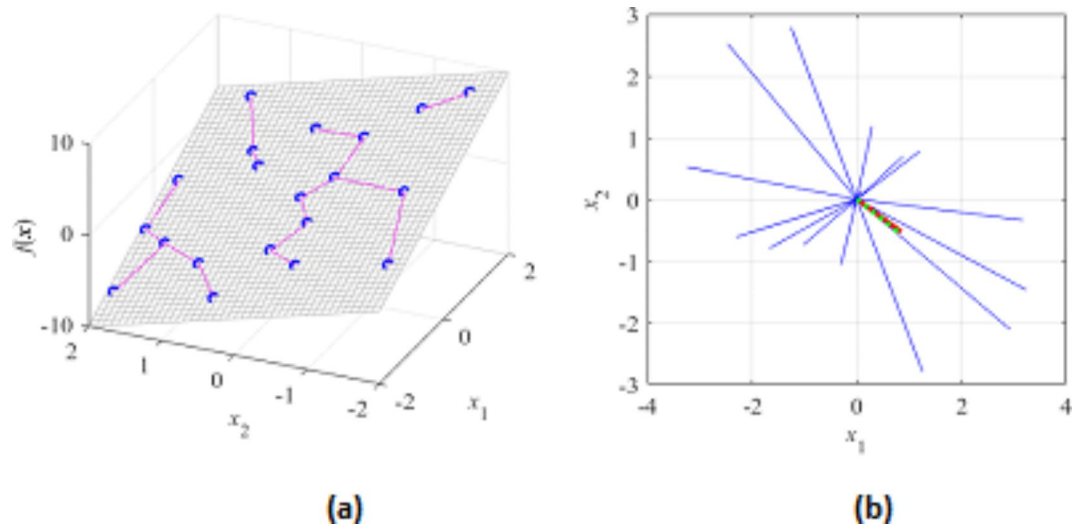
Fig. 6. FGSA illustration using a linear function $f(\boldsymbol{x}) = f([x_1 x_2]^T) = 3x_1 - 2x_2$: (**a**) the surface plot of the function (gray), twenty random observables $\boldsymbol{x}_s^{(k)}$ (circles), and relocation vectors $\boldsymbol{x}_c^{(k)} - \boldsymbol{x}_s^{(k)}$ (line segments); (**b**) relocation matrix vectors $r_s^{(k)} \boldsymbol{v}_s^{(k)}$ (thin lines), the largest principal component $\boldsymbol{e}_1$ (thick solid line), and the normalized gradient $\boldsymbol{g} = [3 - 2]^T / 13^{1/2}$ (thick dotted line). In this example, all function variability occurs along the gradient $\boldsymbol{g}$ (the function is constant in the direction orthogonal to $\boldsymbol{g}$), which is well aligned with the vector $\boldsymbol{e}_1$, obtained using the proposed FGSA.
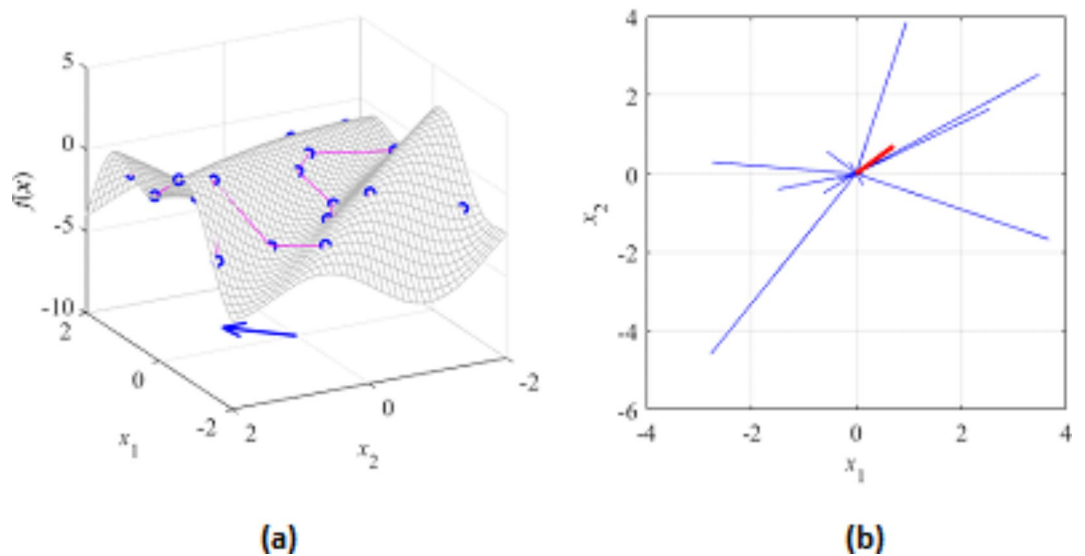

Fig. 7. FGSA illustration using a nonlinear function of two variables: (**a**) surface plot of the first function (gray), twenty random observables $\boldsymbol{x}_s^{(k)}$ (circles), and relocation vectors $\boldsymbol{x}_c^{(k)} - \boldsymbol{x}_s^{(k)}$ (line segments), as well as the principal component $\boldsymbol{e}_1$ (thick arrow); (**b**) relocation matrix vectors $r_s^{(k)} \boldsymbol{v}_s^{(k)}$ (thin lines), and the largest principal component $\boldsymbol{e}_1$ (thick solid line). It can be noticed that the vector $\boldsymbol{e}_1$ obtained using FGSA visually corresponds to the direction of the largest variability of the function $f(\boldsymbol{x})$.

Discussion

This section analyzes the results encapsulated in Tables 6, 7, 8, 9 to evaluate the performance of our technique, also in the light of the benchmark procedures. The following paragraphs summarize our findings regarding the major performance indicators, such as design reliability, design quality, and cost-efficiency.

Optimization process reliability. The acquired numerical data indicates our method's perfect success rate (10/10), i.e., its ability to find satisfactory outcomes in each run and for all test cases. Meanwhile, the results obtained for Algorithm IV (gradient search) underscore that the test problems are multimodal indeed. The average success rate for local optimizer is only 4/10. While nature-inspired optimization (PSO, DE, GWO) fares better, it is still not perfect, which confirms insufficiency of the assumed computational budget. Both machine learning frameworks (Algorithms V and VI) perform consistently with 10/10 success rate; however, Algorithm

12
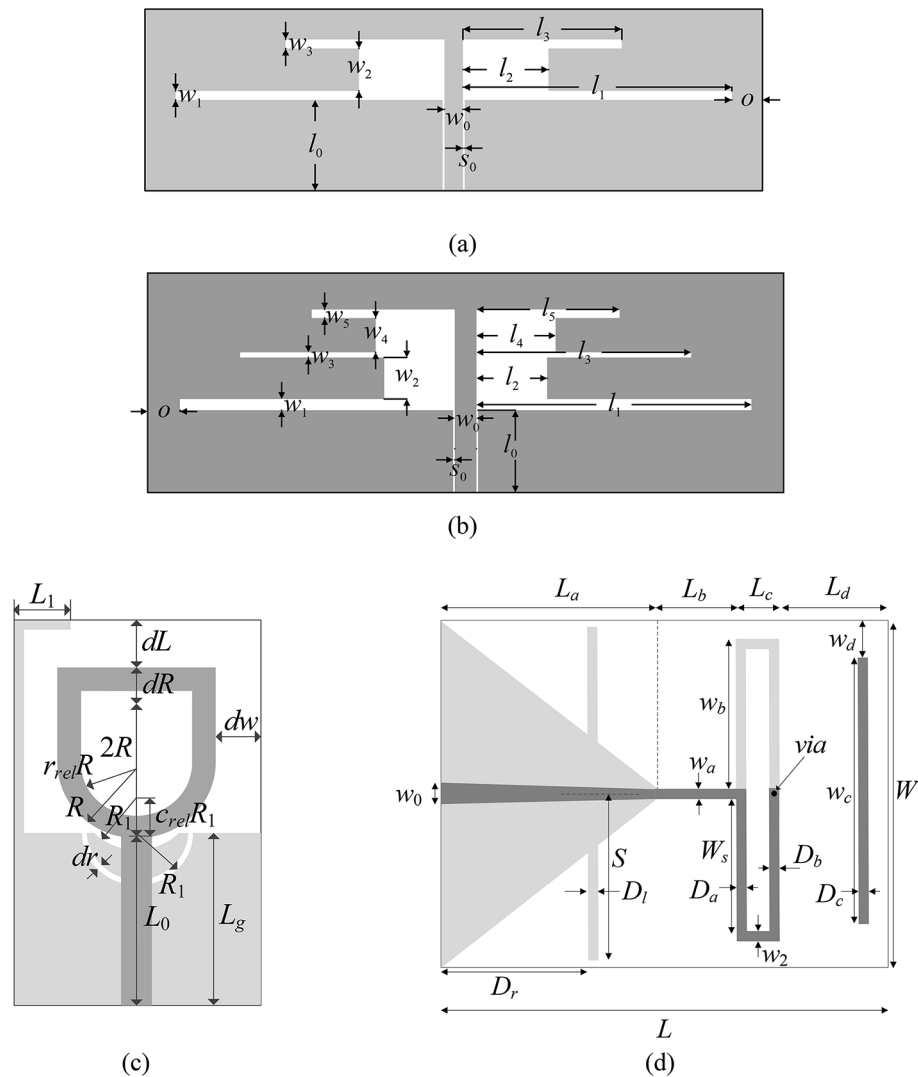
Fig. 8. Test devices: (**a**) Antenna I[129], (**b**) Antenna II[130], (**c**) Antenna III[131], (d) Antenna IV[132]. The light-gray shade is used to indicate the ground-plane metallization.

V does not produce designs of the same quality as Algorithm VI and the proposed technique, which is due to operating in the original parameter space, where building of reliable behavioral models is impeded by the dimensionality-related issues. Also, the computational costs of Algorithms V and VI are significantly higher.

Design quality. This performance figure is evaluated through the mean cost function value. For Antennas I, II, and III, it is the maximum in-band $|S_{11}|$; for Antenna IV it is the end-fire gain at the intended center frequency. The data in Tables 6, 7, 8, 9 shows that the proposed algorithm yields the highest-quality designs, only matched by Algorithm VI. Algorithm V is slightly worse due to operating in the unreduced parameter space and the associated difficulties in surrogate modeling. The quality of results obtained with PSO, DE, and GWO (Algorithms I through III) is noticeably inferior for all antennas, whereas Algorithm IV (gradient search) is clearly inferior due to the fact that—for most runs—local tuning converged to the designs allocated away from the respective optima.

Computational efficiency. The expenses incurred by the search process are remarkably low for the presented technique as compared to all global benchmark procedures (Algorithms I, II, III, V, and VI). In terms of average figures, our framework offers over 54-percent savings over Algorithm VI, 72-percent savings over Algorithm V, and about 90-percent savings over Algorithms I, II, and III. The mean running cost is equivalent to less than 140 high-resolution EM simulations, which is in line with that of gradient-based search (~ 110 EM analyses), while offering the global search capability.

The effects of dimensionality reduction and multi-resolution EM analysis. The impact of dimensionality reduction and the employment of multi-resolution models becomes evident by comparing the performance of the algorithm of section "Variable-resolution machine learning for global antenna optimization using sensitivity-analysis-based dimensionality reduction" with Algorithms V and VI. Operating in the restricted region X_d leads to a noticeable improvement of the design quality and about forty percent cost reduction. The reason behind both is that limiting the global search stage to X_d improves the accuracy of the surrogate operating

Parameter	Antenna structure			
	Antenna I	**Antenna II**	**Antenna III**	**Antenna IV**
Substrate	RO4350 ($\varepsilon_r = 3.5$, $h = 0.76$ mm)	RO4350 ($\varepsilon_r = 3.5$, $h = 0.76$ mm)	RF-35 ($\varepsilon_r = 3.5$, $h = 0.762$ mm)	RO4003 ($\varepsilon_r = 3.38$, $h = 1.5$ mm)
Design parameters$	$x = [l_1 l_2 l_3 w_1 w_2 w_3]^T$	$x = [l_1 l_2 l_{3r}\ l_4 l_{5r}\ w_1 w_2 w_3 w_4 w_5]^T$	$x = [L_0 dR\ R\ r_{rel}\ dL\ dw\ Lg\ L_1 R_1 dr\ c_{rel}]^T$	$x = [L_a\ L_b\ L_c\ L_d\ W\ w_a\ D_a\ D_b\ D_c\ D_{lr}\ D_{rr}\ S_r\ w_{br}\ w_{cr}]^T$
Other parameters$	$l_0 = 30$, $w_0 = 3$, $s_0 = 0.15$, $o = 5$	$l_3 = l_{3r} l_1$ and $l_5 = l_{5r} l_3$; $l_0 = 30$, $w_0 = 3$, $s_0 = 0.15$, $o = 5$	$w_0 = 1.7$	$D_l = D_{lr} L_a$; $D_r = D_{rr} L_a$, $S = S_r W$, $w_b = w_{br} W/2$, $w_c = w_{cr} W$, $w_0 = 3.4$
EM model	CST Microwave Studio	CST Microwave Studio	CST Microwave Studio	CST Microwave Studio
R_c (low-resolution model)	~ 60,000 mesh cells Simulation time 25 s	~ 71,000 mesh cells Simulation time 35 s	~ 210,000 mesh cells Simulation time 51 s	~ 81,000 mesh cells Simulation time 39 s
R_f (high-resolution model)	~ 410,000 mesh cells Simulation time 92 s	~ 270,000 mesh cells Simulation time 80 s	~ 2,300,000 mesh cells Simulation time 424 s	~ 550,000 mesh cells Simulation time 150 s
Target operating frequencies [GHz]	2.45 GHz 5.3 GHz	2.45 GHz 3.6 GHz 5.3 GHz	3.1 GHz to 10.6 GHz	2.5 GHz
Design goals	Minimize reflection at all operating frequencies	Minimize reflection at all operating frequencies	Minimize reflection within the entire UWB band	Maximize realized gain in ± 100 MHz bandwidth centred at f_0; Constraint: $|S_{11}| \leq -10$ dB at the same bandwidth
Parameter space X	$l = [15\ 3\ 0.35\ 0.2\ 1.8\ 0.5]^T$ $u = [50\ 12\ 0.85\ 1.5\ 4.3\ 2.7]^T$	$l = [20\ 3\ 0.6\ 3\ 0.6\ 0.2\ 0.2\ 0.2\ 0.2\ 0.2]^T$ $u = [50\ 5\ 0.85\ 5\ 0.85\ 2.2\ 4.2\ 2.2\ 4.2\ 2.2]^T$	$l = [4.0\ 0.0\ 3.0\ 0.1\ 0.0\ 0.0\ 4.0\ 0.0\ 2.0\ 0.2\ 0.2]^T$ $u = [15.0\ 6.0\ 8.0\ 0.9\ 5.0\ 8.0\ 15.0\ 6.0\ 5.0\ 1.0\ 0.9]^T$	$l = [15\ 5\ 1\ 15\ 25\ 0.5\ 1\ 1.5\ 1.5\ 0.05\ 0.4\ 0.5\ 0.5\ 0.5]^T$ $u = [35\ 25\ 8\ 40\ 60\ 2.5\ 3.0\ 4.5\ 4.5\ 0.25\ 0.9\ 1.0\ 1.0\ 1.0]^T$

Table 4. Verification antenna structures. $Dimensions in mm, except relative one (with subscript r), which are unitless.

Method	Algorithm type	Setup
This work	FGSA-based surrogate-assisted machine-learning framework with dimensionality reduction and variable-resolution EM models	Control parameters: $N_r = 50$, $N_i = 20$, $E_{max} = 20\%$, $\varepsilon = 10^{-2}$, $N_{no\_improve} = 20$, $\varepsilon_{TR} = 10^{-3}$ (see Table 1 for an explanation of terms)
I	Particle swarm optimizer (PSO)	Swarm size $N = 10$, standard control parameters ($\chi = 0.73$, $c_1 = c_2 = 2.05$); the number of iterations set to 50 (version I) and 100 (version II)
II	Differential evolution (DE) [135]	Algorithm setup: • Population size $N = 10$; • Standard control parameters (crossover probability $CR = 0.9$, differential weight $F = 0.8$); Number of iterations set to 100
III	Gray Wolf optimizer (GWO)[37]	Algorithm setup: • Population size $N = 10$; • Standard control parameters, cf.[37]; Number of iterations set to 100
IV	Trust-region gradient-based optimizer[125]	Random initial design, response gradients estimated using finite differentiation, termination criteria based on convergence in argument and reduction of the trust region size[125]
V	Machine-learning procedure	Algorithm setup: • Initial surrogate set up to ensure relative RMS error not higher than 20% with the maximum number of training samples equal to 400; • Algorithm operates in the original parameter space (no dimensionality reduction); • Infill criterion: minimization of the predicted objective function
VI	Machine-learning procedure	Algorithm setup: • The method is the same as the proposed one; however, the algorithm operates at the level of high-resolution EM models; • Control parameters: default values as in Table 1

Table 5. Benchmark algorithms.

within the ML framework and lowers the training data acquisition expenses. The latter is the major contributor to the overall CPU expenses in Algorithm V. On the other hand, utilization of low-resolution EM simulations enabled additional savings (up to the aforementioned 72 percent over Algorithm V). These extra benefits are not detrimental to the design quality. Clearly, the acceleration factor due to variable-resolution modeling is problem dependent as shown in Table 4.

The observations formulated above demonstrate that the proposed variable-resolution machine learning procedure does exhibit global search capability, ensures consistency in terms of producing high-quality designs over multiple algorithm runs and for a variety of design scenarios (optimization of impedance matching, gain enhancement). Its cost efficiency is comparable to local methods, which is perhaps the most essential asset in the context of practical applications. The three fundamental factors contributing to this level of performance include fast sensitivity analysis, dimensionality reduction, and variable-resolution modeling. An additional advantage of the presented technique is that it is easy to set up, which is a consequence of a small number of control parameters.

Optimization algorithm	Performance figure		
	Average objective function value [dB]	Computational cost$	Success rate#
Algorithm I: PSO (50 iterations)	−18.2	500	9/10
Algorithm I: PSO (100 iterations)	−19.3	1000	10/10
Algorithm II: DE (100 iterations)	−19.8	1000	9/10
Algorithm III: GWO (100 iterations)	−19.1	1000	9/10
Algorithm IV: Trust-region gradient-based algorithm	−13.5	84.2	6/10
Algorithm V: Machine learning operating in the original parameter space X	−20.7	457.8	10/10
Algorithm VI: FSGA-based machine learning operating at the level of high-resolution model only	−20.6	221.8	10/10
Proposed algorithm	−24.5	104.8	10/10

Table 6. Antenna I: optimization results. $The cost expressed in terms of the number of EM simulations of the antenna structure under design. #Number of algorithms runs at which the operating frequencies were allocated in the vicinity of the target frequencies.

| Optimization algorithm	Performance figure		
	Average objective function value [dB]	Computational cost$	Success rate#
Algorithm I: PSO (50 iterations)	−10.8	500	5/10
Algorithm I: PSO (100 iterations)	−13.8	1000	8/10
Algorithm II: DE (100 iterations)	−12.5	1000	8/10
Algorithm III: GWO (100 iterations)	−11.3	1000	7/10
Algorithm IV: Trust-region gradient-based algorithm	−7.8	105.8	4/10
Algorithm V: Machine learning operating in the original parameter space X	−13.5	470.0	10/10
Algorithm VI: FSGA-based machine learning operating at the level of high-resolution model only	−15.4	303.7	10/10
Proposed algorithm	−17.7	192.3	10/10

Table 7. Antenna II: optimization results. $The cost expressed in terms of the number of EM simulations of the antenna structure under design. #Number of algorithms runs at which the operating frequencies were allocated in the vicinity of the target frequencies.

Optimization algorithm	Performance figure		
	Average objective function value [dB]	Computational cost$	Success rate#
Algorithm I: PSO (50 iterations)	−12.3	500	9/10
Algorithm I: PSO (100 iterations)	−12.6	1000	10/10
Algorithm II: DE (100 iterations)	−12.7	1000	10/10
Algorithm III: GWO (100 iterations)	−11.9	1000	9/10
Algorithm IV: Trust-region gradient-based algorithm	−7.8	99.2	5/10
Algorithm V: Machine learning operating in the original parameter space X	−11.8	471.6	9/10
Algorithm VI: FSGA-based machine learning operating at the level of high-resolution model only	−13.2	308.1	10/10
Proposed algorithm	−13.1	79.8	10/10

Table 8. Antenna III: optimization results. $The cost expressed in terms of the number of EM simulations of the antenna structure under design. #Number of algorithms runs at which the maximum in-band matching was reduced below −10 dB.

Conclusion

The presented study aimed at developing a two-stage methodology for global design optimization of antenna systems. Its keystone components include dimensionality reduction realized by means of fast global sensitivity analysis (FGSA), a machine learning (ML) procedure involving kriging surrogate models, and fine tuning of antenna parameters using accelerated trust-region (TR) search. Restricting the ML process to the FGSA-defined low-dimensionality domain facilitates the construction and refinement of the surrogate model, which is further expedited by conducting this stage using low-resolution EM simulations. On the other hand, the final tuning is carried out in the full-dimensionality space and using high-resolution EM analysis, which ensures the reliability of the optimization process. Extensive verification experiments involved four antennas of diverse

| Optimization algorithm	Performance figure		
	Average objective function value [dB][&]	Computational cost[$]	Success rate[#]
Algorithm I: PSO (50 iterations)	6.1	500	9/10
Algorithm I: PSO (100 iterations)	6.8	1000	10/10
Algorithm II: DE (100 iterations)	7.0	1000	10/10
Algorithm III: GWO (100 iterations)	6.8	1000	10.10
Algorithm IV: Trust-region gradient-based algorithm	− 1.1	144.3	1/10
Algorithm V: Machine learning operating in the original parameter space X	7.9	583.3	10/10
Algorithm VI: FSGA-based machine learning operating at the level of high-resolution model only	8.0	370.4	10/10
Proposed algorithm	8.1	173.3	10/10

Table 9. Antenna IV: optimization results. [&]The values reported in the table refer to the realized gain at the target operating frequency of 2.5 GHz. [$]The cost expressed in terms of the number of EM simulations of the antenna structure under design. [#]Number of algorithms runs at which the operating frequencies were allocated in the vicinity of the target frequency.
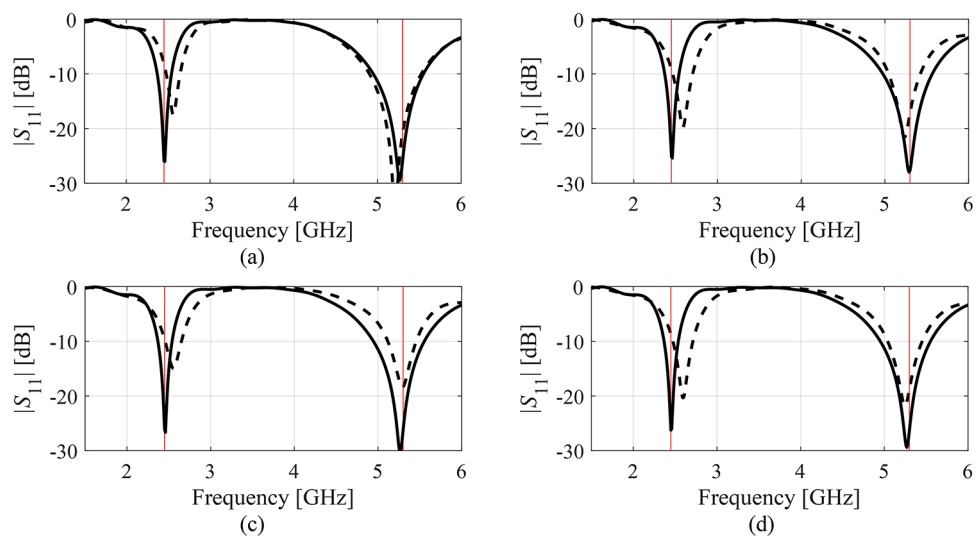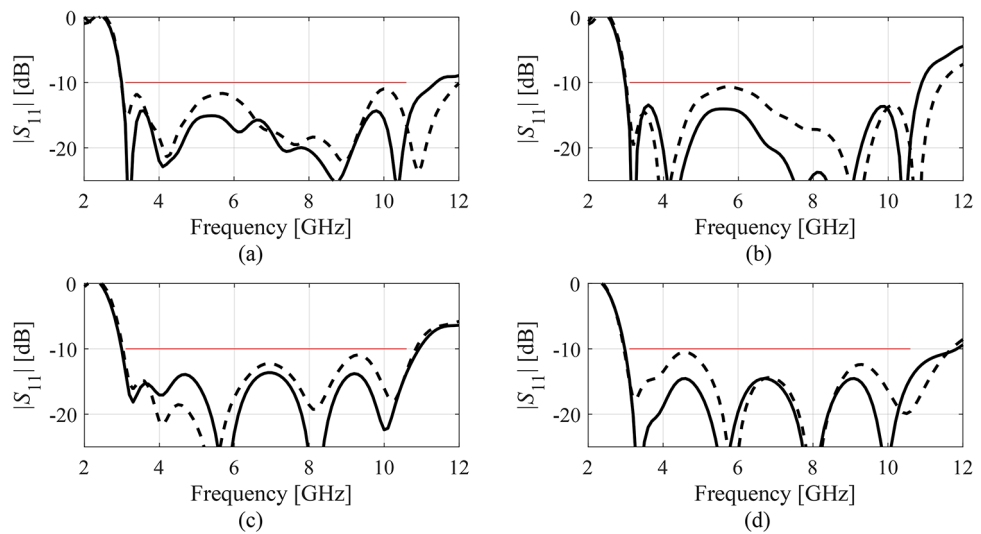

Fig. 9. $|S_{11}|$ of Antenna I at the designs produced by the proposed variable-resolution surrogate-assisted machine learning framework. Shown is the data for selected algorithm runs (plots (**a**) through (**d**)). The design $x^{(0)}$ generated by the global optimization step (- - -) and the final design (—). Target operating frequencies marked with vertical lines.

responses (multi-band, broadband, enhanced gain). The results demonstrate consistent operation, reliability, repeatability of solutions, and excellent cost efficiency of the presented framework. It is superior to several benchmark approaches that include nature-inspired procedures and machine-learning strategies. The average running expenses of the algorithm correspond to only about 140 EM antenna simulations, which is comparable to the expenses incurred by local optimization. The computational savings due to dimensionality reduction are over fifty percent with the additional advantage being improved design quality. The incorporation of variable-resolution models results in further speedup (over seventy-percent savings over the baseline ML). Other features of the proposed technique include straightforward setup, and a small number of control parameters, due to which there is no need for tuning the procedure to a given optimization problem. Altogether, our framework can be considered an attractive solution approach to antenna optimization tasks, especially when global search capability is necessary and the computational budget is limited.
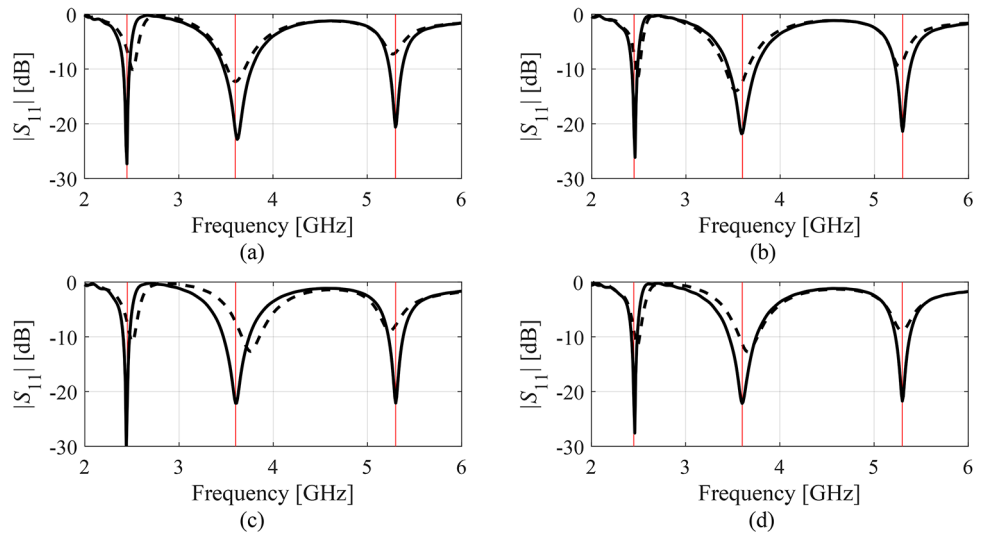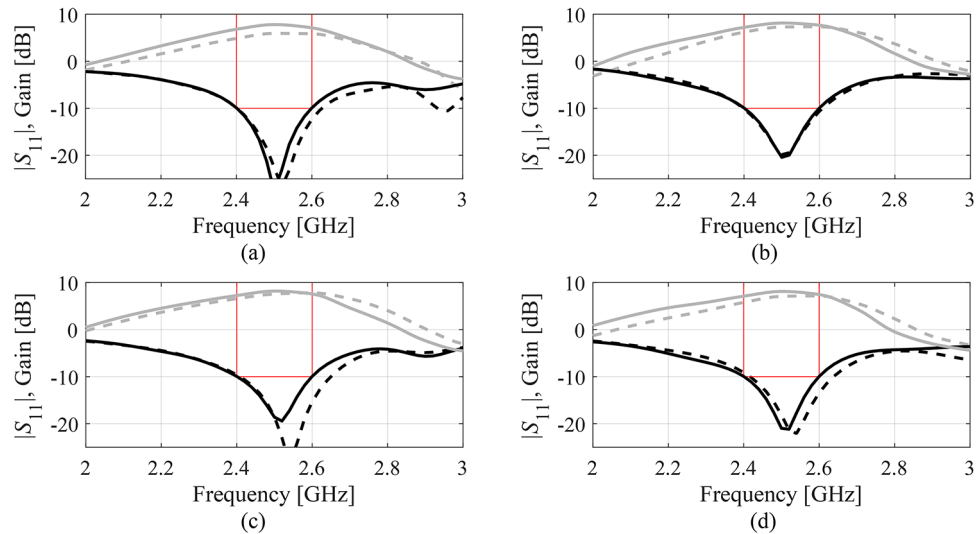
Fig. 10. $|S_{11}|$ of Antenna II at the designs produced by the proposed variable-resolution surrogate-assisted machine learning framework. Shown is the data for selected algorithm runs (plots (**a**) through (**d**)). The design $x^{(0)}$ generated by the global optimization step (- - -) and the final design (—). Target operating frequencies marked with vertical lines.

Fig. 11. $|S_{11}|$ of Antenna III at the designs produced by the proposed variable-resolution surrogate-assisted machine learning framework. Shown is the data for selected algorithm runs (plots (**a**) through (**d**)). The design $x^{(0)}$ generated by the global optimization step (- - -) and the final design (—). Target operating bandwidth marked with the horizontal line.

Fig. 12. $|S_{11}|$ and realized gain of Antenna IV at the designs produced by the proposed variable-resolution surrogate-assisted machine learning framework. Shown is the data for selected algorithm runs (plots (**a**) through (**d**)). The design $x^{(0)}$ generated by the global optimization step (- - -) and the final design (—). Target operating bandwidth marked with the horizontal line placed at the acceptance level of −10 dB for $|S_{11}|$.

Data availability

The datasets used and/or analyzed during the current study available from the corresponding author on reasonable request.

References

1. Zhang, Y., Deng, J., Li, M., Sun, D. & Guo, L. A MIMO dielectric resonator antenna with improved isolation for 5G mm-wave applications. *IEEE Antennas Wirel. Propag. Lett.* **18**(4), 747–751 (2019).
2. Wen, S. & Dong, Y. A low-profile wideband antenna with monopolelike radiation characteristics for 4G/5G indoor micro base station application. *IEEE Antennas Wirel. Propag. Lett.* **19**(12), 2305–2309 (2020).
3. Jha, K. R., Bukhari, B., Singh, C., Mishra, G. & Sharma, S. K. Compact planar multistandard MIMO antenna for IoT applications. *IEEE Trans. Antennas Propag.* **66**(7), 3327–3336 (2018).
4. Lin, X. et al. Ultrawideband textile antenna for wearable microwave medical imaging applications. *IEEE Trans. Antennas Propag.* **68**(6), 4238–4249 (2020).
5. Kapusuz, K. Y., Berghe, A. V., Lemey, S. & Rogier, H. Partially filled half-mode substrate integrated waveguide leaky-wave antenna for 24 GHz automotive radar. *IEEE Antennas Wirel. Propag. Lett.* **20**(1), 33–37 (2021).
6. Mansour, M. M. & Kanaya, H. High-efficient broadband CPW RF rectifier for wireless energy harvesting. *IEEE Microw. Wirel. Comp. Lett.* **29**(4), 288–290 (2019).
7. Erman, F., Koziel, S., Hanafi, E., Soboh, R. & Szczepanski, S. Miniaturized metal-mountable U-shaped inductive-coupling-fed UHF RFID tag antenna with defected microstrip surface. *IEEE Access* **10**, 47301–47308 (2022).
8. He, Y., Yue, Y., Zhang, L. & Chen, Z. N. A dual-broadband dual-polarized directional antenna for all-spectrum access base station applications. *IEEE Trans. Antennas Propag.* **69**(4), 1874–1884 (2021).
9. Sun, L., Li, Y., Zhang, Z. & Feng, Z. Wideband 5G MIMO antenna with integrated orthogonal-mode dual-antenna pairs for metal-rimmed smartphones. *IEEE Trans. Antennas Propag.* **68**(4), 2494–2503 (2020).
10. Sung, Y. Simple slot antenna with polarization diversity. *IEEE Antennas Wirel. Propag. Lett.* **21**(4), 690–694 (2022).
11. Xu, H.-X. et al. Polarization-insensitive metalens and its applications to reflectarrays with polarization diversity. *IEEE Trans. Antennas Propag.* **70**(3), 1895–1905 (2022).
12. Hynes, C. G. & Vaughan, R. G. Conical monopole antenna with integrated tunable notch filters. *IEEE Antennas Wirel. Propag. Lett.* **19**(12), 2398–2402 (2020).
13. Rabbani, M. S., Churm, J. & Feresidis, A. P. Continuous beam-steering low-loss millimeter-wave antenna based on a piezo-electrically actuated metasurface. *IEEE Trans. Antennas Propag.* **70**(4), 2439–2449 (2022).
14. Farahat, A. E., Hussein, K. F. A. & El-Hassan, M. A. Design methodology of multiband printed antennas for future generations of mobile handsets. *IEEE Access* **10**, 75918–75931 (2022).
15. Chen, C. A compact wideband endfire filtering antenna inspired by a uniplanar microstrip antenna. *IEEE Antennas Wirel. Propag. Lett.* **21**(4), 853–857 (2022).
16. Chen, Z. et al. Compact wideband circularly polarized loop antenna based on dual common and differential modes. *IEEE Antennas Wirel. Propag. Lett.* **21**(8), 1567–1571 (2022).
17. Nagaraju, D. & Verma, Y. K. A compact conformal stub-loaded long slot leaky-wave antenna with wide beamwidth. *IEEE Antennas Wirel. Propag. Lett.* **20**(6), 953–957 (2021).
18. Sun, L., Li, Y. & Zhang, Z. Wideband dual-polarized endfire antenna based on compact open-ended cavity for 5G mm-wave mobile phones. *IEEE Trans. Antennas Propag.* **70**(3), 1632–1642 (2022).
19. Chen, X., Tang, M.-C., Yi, D. & Ziolkowski, R. W. Wideband, compact antennas with interdigitated magnetic-based near-field resonant parasitic elements. *IEEE Trans. Antennas Propag.* **69**(8), 5036–5041 (2021).
20. Cicchetti, R., Cicchetti, V., Faraone, A., Foged, L. & Testa, O. A compact high-gain wideband lens Vivaldi antenna for wireless communications and through-the-wall imaging. *IEEE Trans. Antennas Propag.* **69**(6), 3177–3192 (2021).

18

21. Liu, Y. & Yagoub, M. C. E. Compact omnidirectional millimeter-wave antenna array fed in series by a novel feed network. *IEEE Trans. Antennas Propag.* **69**(11), 7604–7612 (2021).
22. Hu, H. et al. Compact planar inverted-F antenna for MicroSats omnidirectional communications. *IEEE Antennas Wirel. Propag. Lett.* **20**(2), 160–164 (2021).
23. Podilchak, S. K., Johnstone, J. C., Caillet, M., Clénet, M. & Antar, Y. M. M. A compact wideband dielectric resonator antenna with a meandered slot ring and cavity backing. *IEEE Antennas Wirel. Propag. Lett.* **15**, 909–913 (2016).
24. Hu, W., Yin, Y., Yang, X. & Fei, P. Compact multiresonator-loaded planar antenna for multiband operation. *IEEE Trans. Antennas Propag.* **61**(5), 2838–2841 (2013).
25. Haq, M. A., Koziel, S. & Cheng, Q. S. Miniaturization of wideband antennas by means of feed line topology alterations. *IET Microw. Antennas Propag.* **12**(13), 2128–2134 (2018).
26. Ding, Z., Jin, R., Geng, J., Zhu, W. & Liang, X. Varactor loaded pattern reconfigurable patch antenna with shorting pins. *IEEE Trans. Antennas Propag.* **67**(10), 6267–6277 (2019).
27. Zhu, S., Liu, H., Wen, P., Chen, Z. & Xu, H. Vivaldi antenna array using defected ground structure for edge effect restraint and back radiation suppression. *IEEE Antennas Wirel. Propag. Lett.* **19**(1), 84–88 (2020).
28. Gallardo, D., Monasterio, D., Finger, R., Mena, F. P. & Bronfman, L. A compact metamaterial-based antenna for multiband phased array applications. *IEEE Trans. Antennas Propag.* **69**(12), 8872–8877 (2021).
29. Priya, S., Dwari, S., Kumar, K. & Mandal, M. K. Compact self-quadruplexing SIW cavity-backed slot antenna. *IEEE Trans. Antennas Propag.* **67**(10), 6656–6660 (2019).
30. Li, W.-Y., Chung, W., Hsiao, F.-R., Li, T.-L., Kao, T.-H. & Huang, M.-C. Compact multi-layer handset phone 13.56 MHz NFC antenna design by novel laser-induced thin-film antenna (LITA) technologies. *Int. Symp. Antennas Propag. (ISAP)*, pp. 26–27, 24–28 Oct., Okinawa (2016).
31. Iqbal, A., Al-Hasan, M., Mabrouk, I. B. & Nedil, M. Ultracompact quarter-mode substrate integrated waveguide self-diplexing antenna. *IEEE Antennas Wirel. Propag. Lett.* **20**(7), 1269–1273 (2021).
32. Zhang, Y., Yang, W., Xue, Q., Huang, J. & Che, W. Broadband dual-polarized differential-fed filtering antenna array for 5G millimeter-wave applications. *IEEE Trans. Antennas Propag.* **70**(3), 1989–1998 (2022).
33. Ullah, U., Al-Hasan, M., Koziel, S. & Ben Mabrouk, I. EM-driven size reduction and multi-criterial optimization of broadband circularly-polarized antennas using Pareto front traversing and design extrapolation. *Sci. Rep.* **12**, 9877 (2022).
34. Koziel, S. & Pietrenko-Dabrowska, A. On EM-driven size reduction of antenna structures with explicit constraint handling. *IEEE Access* **9**, 165766–165772 (2021).
35. Chen, M.-N., Lu, W.-J., Wang, L.-J., Yang, M. & Zhu, L. Design approach to a novel planar bisensing circularly polarized antenna. *IEEE Trans. Antennas Propag.* **67**(11), 6839–6846 (2019).
36. Cuevas, M., Pizarro, F., Leiva, A., Hermosilla, G. & Yunge, D. Parametric study of a fully 3D-printed dielectric resonator antenna loaded with a metallic cap. *IEEE Access* **9**, 73771–73779 (2021).
37. Li, X. & Luk, K. M. The grey wolf optimizer and its applications in electromagnetics. *IEEE Trans. Antennas Propag.* **68**(3), 2186–2197 (2020).
38. Luo, X., Yang, B. & Qian, H. J. Adaptive synthesis for resonator-coupled filters based on particle swarm optimization. *IEEE Trans. Microw. Theory Technol.* **67**(2), 712–725 (2019).
39. Majumder, A., Chatterjee, S., Chatterjee, S., Sinha Chaudhari, S. & Poddar, D. R. Optimization of small-signal model of GaN HEMT by using evolutionary algorithms. *IEEE Microw. Wirel. Comp. Lett.* **27**(4), 362–364 (2017).
40. Liang, S. et al. Sidelobe reductions of antenna arrays via an improved chicken swarm optimization approach. *IEEE Access* **8**, 37664–37683 (2020).
41. Tang, M., Chen, X., Li, M. & Ziolkowski, R. W. Particle swarm optimized, 3-D-printed, wideband, compact hemispherical antenna. *IEEE Antennas Wirel. Propag. Lett.* **17**(11), 2031–2035 (2018).
42. Liu, F., Liu, Y., Han, F., Ban, Y.-L. & Jay Guo, Y. Synthesis of large unequally spaced planar arrays utilizing differential evolution with new encoding mechanism and Cauchy mutation. *IEEE Trans. Antennas Propag.* **68**(6), 4406–4416 (2020).
43. Li, W., Zhang, Y. & Shi, X. Advanced fruit fly optimization algorithm and its application to irregular subarray phased array antenna synthesis. *IEEE Access* **7**, 165583–165596 (2019).
44. Al-Azza, A. A., Al-Jodah, A. A. & Harackiewicz, F. J. Spider monkey optimization: a novel technique for antenna optimization. *IEEE Antennas Wirel. Propag. Lett.* **15**, 1016–1019 (2016).
45. Afsari, A., Abbosh, A. M. & Rahmat-Samii, Y. Adaptive beamforming by compact arrays using evolutionary optimization of Schelkunoff polynomials. *IEEE Trans. Antennas Propag.* **70**(6), 4485–4497 (2022).
46. Rocca, P., Poli, L., Anselmi, N. & Massa, A. Nested optimization for the synthesis of asymmetric shaped beam patterns in subarrayed linear antenna arrays. *IEEE Trans. Antennas Propag.* **70**(5), 3385–3397 (2022).
47. Genovesi, S., Mittra, R., Monorchio, A. & Manara, G. Particle swarm optimization for the design of frequency selective surfaces. *IEEE Antennas Wirel. Propag. Lett.* **5**, 277–279 (2006).
48. Koziel, S. & Abdullah, M. Machine-learning-powered EM-based framework for efficient and reliable design of low scattering metasurfaces. *IEEE Trans. Microw. Theory Technol.* **69**(4), 2028–2041 (2021).
49. Koziel, S. & Pietrenko-Dabrowska, A. Reliable EM-driven size reduction of antenna structures by means of adaptive penalty factors. *IEEE Trans. Antennas Propag.* **70**(2), 1389–1401 (2021).
50. Mahrokh, M. & Koziel, S. Explicit size-reduction of circularly polarized antennas through constrained optimization with penalty factor adaptation. *IEEE Access* **9**, 132390–132396 (2021).
51. Koziel, S. & Pietrenko-Dabrowska, A. Expedited acquisition of database designs for reduced-cost performance-driven modeling and rapid dimension scaling of antenna structures. *IEEE Trans. Antennas Propag.* **69**(8), 4975–4987 (2021).
52. Bora, T. C., Lebensztajn, L. & Coelho, L. D. S. Non-dominated sorting genetic algorithm based on reinforcement learning to optimization of broad-band reflector antennas satellite. *IEEE Trans. Magn.* **48**(2), 767–770 (2012).
53. Ding, D. & Wang, G. Modified multiobjective evolutionary algorithm based on decomposition for antenna design. *IEEE Trans. Antennas Propag.* **61**(10), 5301–5307 (2013).
54. Yang, C., Zhang, J. & Tong, M. S. An FFT-accelerated particle swarm optimization method for solving far-field inverse scattering problems. *IEEE Trans. Antennas Propag.* **69**(2), 1078–1093 (2021).
55. Liu, X., Du, B., Zhou, J. & Xie, L. Optimal design of elliptical beam cassegrain antenna. *IEEE Access* **9**, 120765–120773 (2021).
56. Braik, M., Hammouri, A., Atwan, J., Al-Betar, M. A. & Awadallah, M. A. White Shark Optimizer: A novel bio-inspired meta-heuristic algorithm for global optimization problems. *Knowl. Based Syst.* **243**, 108457 (2022).
57. Houssein, E. H., Hosney, M. E., Oliva, D., Younis, E. M. G., Ali, A. A. & Mohamed, W. M. An efficient discrete rat swarm optimizer for global optimization and feature selection in chemoinformatics. *Knowl. Based Syst.* **275**, 110697 (2023).
58. Kumar, S., Yildiz, B. S., Mehta, P., Panagant, N., Sait, S. M., Mirjalili, S. & Yildiz, A. R. Chaotic marine predators algorithm for global optimization of real-world engineering problems. *Knowl.-Based Syst.* **261**, 110192 (2023).
59. Zhang, Q., Gao, H., Zhan, Z. H., Li, J. & Zhang, H. Growth Optimizer: A powerful metaheuristic algorithm for solving continuous and discrete global optimization problems. *Knowl.-Based Syst.* **261**, 110206 (2023).
60. Mostafa, R. R., Gaheen, M. A., ElAziz, M. A., Al-Betar, M. A. & Ewees, A. A. An improved gorilla troops optimizer for global optimization problems and feature selection. *Knowl.-Based Syst.* **269**, 110462 (2023).
61. Abdel-Salam, M., Alzahrani, A. I., Alblehai, F., Abu Zitar, R. & Abualigah, L. An improved genghis khan optimizer based on enhanced solution quality strategy for global optimization and feature selection problems. *Knowl.-Based Syst.*, 112237 (2024).

AQ1

62. Goldberg, D. E. & Holland, J. H. *Genetic Algorithms and Machine Learning* (Springer, 1988).
63. Michalewicz, Z. *Genetic Algorithms + Data Structures = Evolution Programs* (Springer, 1996).
64. Choi, K., Jang, D., Kang, S., Lee, J., Chung, T. & Kim, H. Hybrid algorithm combing genetic algorithm with evolution strategy for antenna design. *IEEE Trans. Magn.* **52**(3), 1–4, 7209004 (2016).
65. Wang, D., Tan, D. & Liu, L. Particle swarm optimization algorithm: an overview. *Soft Comput.* **22**, 387–408 (2018).
66. Jiang, Z. J., Zhao, S., Chen, Y. & Cui, T. J. Beamforming optimization for time-modulated circular-aperture grid array with DE algorithm. *IEEE Antennas Wirel. Propag. Lett.* **17**(12), 2434–2438 (2018).
67. Baumgartner, P., Baurnfeind, T., Biro, O., Hackl, A., Magele, C., Renhart, W. & Torchio, R. Multi-objective optimization of Yagi-Uda antenna applying enhanced firefly algorithm with adaptive cost function. *IEEE Trans. Magn.* **54**(3), 8000504 (2018).
68. Yang, S. H. & Kiang, J. F. Optimization of sparse linear arrays using harmony search algorithms. *IEEE Trans. Antennas Propag.* **63**(11), 4732–4738 (2015).
69. Xu, Q., Zeng, S., Zhao, F., Jiao, R. & Li, C. On formulating and designing antenna arrays by evolutionary algorithms. *IEEE Trans. Antennas Propag.* **69**(2), 1118–1129 (2021).
70. Zhu, D. Z., Werner, P. L. & Werner, D. H. Design and optimization of 3-D frequency-selective surfaces based on a multiobjective lazy ant colony optimization algorithm. *IEEE Trans. Antennas Propag.* **65**(12), 7137–7149 (2017).
71. Zheng, T. et al. IWORMLF: improved invasive weed optimization with random mutation and Lévy flight for beam pattern optimizations of linear and circular antenna arrays. *IEEE Access* **8**, 19460–19478 (2020).
72. Tang, W. J., Li, M. S., Wu, Q. H. & Saunders, J. R. Bacterial foraging algorithm for optimal power flow in dynamic environments. *IEEE Trans. Circ. Syst. I Regul. Pap.* **55**(8), 2433–2442 (2008).
73. Prabhakar, S. K., Rajaguru, H. & Lee, S. A framework for schizophrenia EEG signal classification with nature inspired optimization algorithms. *IEEE Access* **8**, 39875–39897 (2020).
74. Darvish, A. & Ebrahimzadeh, A. Improved fruit-fly optimization algorithm and its applications in antenna arrays synthesis. *IEEE Trans. Antennas Propag.* **66**(4), 1756–1766 (2018).
75. Oyelade, O. N., Ezugwu, A.E.-S., Mohamed, T. I. A. & Abualigah, L. Ebola optimization search algorithm: a new nature-inspired metaheuristic optimization algorithm. *IEEE Access* **10**, 16150–16177 (2022).
76. Yang, X. S. Nature-inspired optimization algorithms: challenges and open problems. *J. Comput. Sci.* **46**, 101104 (2020).
77. He, X. et al. Distributed evolution strategies for black-box stochastic optimization. *IEEE Trans. Parallel Distrib. Comput. Syst.* **33**(12), 3718–3731 (2022).
78. Queipo, N. V. et al. Surrogate-based analysis and optimization. *Prog. Aerosp. Sci.* **41**(1), 1–28 (2005).
79. Easum, J. A., Nagar, J., Werner, P. L. & Werner, D. H. Efficient multi-objective antenna optimization with tolerance analysis through the use of surrogate models. *IEEE Trans. Antennas Propag.* **66**(12), 6706–6715 (2018).
80. Koziel, S. & Pietrenko-Dabrowska, A. Rapid multi-objective optimization of antennas using nested kriging surrogates and single-fidelity EM simulation models. *Eng. Comput.* **37**(4), 1491–1512 (2019).
81. Liu, J., Dong, H. & Wang, P. Multi-fidelity global optimization using a data-mining strategy for computationally intensive black-box problems. *Knowl.-Based Syst.* **227**, 107212 (2021).
82. Hu, C., Zeng, S. & Li, C. A framework of global exploration and local exploitation using surrogates for expensive optimization. *Knowl.-Based Syst.* **280**, 11018 (2023).
83. de Villiers, D. I. L., Couckuyt, I. & Dhaene, T. Multi-objective optimization of reflector antennas using kriging and probability of improvement. *Int. Symp. Antennas Propag.*, 985–986 (2017).
84. Dong, J., Qin, W. & Wang, M. Fast multi-objective optimization of multi-parameter antenna structures based on improved BPNN surrogate model. *IEEE Access* **7**, 77692–77701 (2019).
85. Jacobs, J. P. Characterization by Gaussian processes of finite substrate size effects on gain patterns of microstrip antennas. *IET Microw. Antennas Propag.* **10**(11), 1189–1195 (2016).
86. Wu, Q., Wang, H. & Hong, W. Multistage collaborative machine learning and its application to antenna modeling and optimization. *IEEE Trans. Antennas Propag.* **68**(5), 3397–3409 (2020).
87. Forrester, A. I. J. & Keane, A. J. Recent advances in surrogate-based optimization. *Prog. Aerosp. Sci.* **45**, 50–79 (2009).
88. Couckuyt, I., Declercq, F., Dhaene, T., Rogier, H. & Knockaert, L. Surrogate-based infill optimization applied to electromagnetic problems. *Int. J. RF Microw. Comput.-Aided Eng.* **20**(5), 492–501 (2010).
89. Alzahed, A. M., Mikki, S. M. & Antar, Y. M. M. Nonlinear mutual coupling compensation operator design using a novel electromagnetic machine learning paradigm. *IEEE Antennas Wirel. Propag. Lett.* **18**(5), 861–865 (2019).
90. Tak, J., Kantemur, A., Sharma, Y. & Xin, H. A 3-D-printed W-band slotted waveguide array antenna optimized using machine learning. *IEEE Antennas Wirel. Propag. Lett.* **17**(11), 2008–2012 (2018).
91. Torun, H. M. & Swaminathan, M. High-dimensional global optimization method for high-frequency electronic design. *IEEE Trans. Microw. Theory Technol.* **67**(6), 2128–2142 (2019).
92. Xia, B., Ren, Z. & Koh, C. S. Utilizing kriging surrogate models for multi-objective robust optimization of electromagnetic devices. *IEEE Trans. Magn.* **50**(2), 7017104 (2014).
93. Taran, N., Ionel, D. M. & Dorrell, D. G. Two-level surrogate-assisted differential evolution multi-objective optimization of electric machines using 3-D FEA. *IEEE Trans. Magn.* **54**(11), 8107605 (2018).
94. Lv, Z., Wang, L., Han, Z., Zhao, J. & Wang, W. Surrogate-assisted particle swarm optimization algorithm with Pareto active learning for expensive multi-objective optimization. *IEEE/CAA J. Autom. Sin.* **6**(3), 838–849 (2019).
95. Koziel, S. Low-cost data-driven surrogate modeling of antenna structures by constrained sampling. *IEEE Antennas Wirel. Propag. Lett.* **16**, 461–464 (2017).
96. Koziel, S. & Sigurdsson, A. T. Triangulation-based constrained surrogate modeling of antennas. *IEEE Trans. Antennas Propag.* **66**(8), 4170–4179 (2018).
97. Koziel, S. & Pietrenko-Dabrowska, A. Performance-based nested surrogate modeling of antenna input characteristics. *IEEE Trans. Antennas Propag.* **67**(5), 2904–2912 (2019).
98. Koziel, S. & Pietrenko-Dabrowska, A. *Performance-Driven Surrogate Modeling of High-Frequency Structures* (Springer, 2020).
99. Pietrenko-Dabrowska, A. & Koziel, S. Antenna modeling using variable-fidelity EM simulations and constrained co-kriging. *IEEE Access* **8**(1), 91048–91056 (2020).
100. Pietrenko-Dabrowska, A., Koziel, S. & Ullah, U. Reduced-cost two-level surrogate antenna modeling using domain confinement and response features. *Sci. Rep.* **12**, 4667 (2022).
101. Koziel, S. Fast simulation-driven antenna design using response-feature surrogates. *Int. J. RF Microw. CAE* **25**(5), 394–402 (2015).
102. Koziel, S. & Bandler, J. W. Reliable microwave modeling by means of variable-fidelity response features. *IEEE Trans. Microw. Theory Tech.* **63**(12), 4247–4254 (2015).
103. Pietrenko-Dabrowska, A. & Koziel, S. Generalized formulation of response features for reliable optimization of antenna input characteristics. *IEEE Trans. Antennas Propag.* **70**(5), 3733–3748 (2021).
104. Marler, R. T. & Arora, J. S. The weighted sum method for multi-objective optimization: new insights. *Struct. Multidiscip. Opt.* **41**, 853–862 (2010).
105. Koziel, S., Pietrenko-Dabrowska, A. & Mahrokh, M. On decision-making strategies for improved-reliability size reduction of microwave passives: intermittent correction of equality constraints and adaptive handling of inequality constraints. *Knowl.-Based Syst.* (2022).

106. Cervantes-González, J. C. et al. Space mapping optimization of handset antennas considering EM effects of mobile phone components and human body. *Int. J. RF Microw. CAE* **26**(2), 121–128 (2016).
107. Koziel, S. & Ogurtsov, S. *Antenna Design by Simulation-Driven Optimization. Surrogate-Based Approach* (Springer, 2014).
108. Koziel, S., Pietrenko-Dabrowska, A. & Plotka, P. Reduced-cost microwave design closure by multi-resolution EM simulations and knowledge-based model management. *IEEE Access* **9**, 116326–116337 (2021).
109. Koziel, S. & Bandler, J. W. A space-mapping approach to microwave device modeling exploiting fuzzy systems. *IEEE Trans. Microw. Theory Tech.* **55**(12), 2539–2547 (2007).
110. Pietrenko-Dabrowska, A. & Koziel, S. Surrogate modeling of impedance matching transformers by means of variable-fidelity EM simulations and nested co-kriging. *Int. J. RF Microw. CAE* **30**(8), e22268 (2020).
111. Liu, B., Koziel, S. & Ali, N. SADEA-II: a generalized method for efficient global optimization of antenna design. *J. Comput. Des. Eng.* **4**(2), 86–97 (2017).
112. Pietrenko-Dabrowska, A. & Koziel, S. Accelerated gradient-based optimization of antenna structures using multi-fidelity simulation models. *IEEE Trans. Antennas Propag.* **69**(12), 8778–8789 (2021).
113. Koziel, S. & Pietrenko-Dabrowska, A. Cost-efficient performance-driven modeling of multi-band antennas by variable-fidelity EM simulations and customized space mapping. *Int. J. Numer. Model.* **33**(6), e2778 (2020).
114. Iooss, B. & Lemaitre, P. A review on global sensitivity analysis methods. In *Uncertainty Management in Simulation-Optimization of Complex Systems* (eds Dellino, G. & Meloni, C.) 101–122 (Springer, 2015).
115. Tian, W. A review of sensitivity analysis methods in building energy analysis. *Renew. Sustain. Energy Rev.* **20**, 411–419 (2013).
116. Morris, M. D. Factorial sampling plans for preliminary computational experiments. *Technometrics* **33**, 161–174 (1991).
117. Saltelli, A. Making best use of model evaluations to compute sensitivity indices. *Comput. Phys. Commun.* **145**, 280–297 (2002).
118. Kovacs, I., Topa, M., Buzo, A., Rafaila, M. & Pelz, G. Comparison of sensitivity analysis methods in high-dimensional verification spaces. *Acta Tec. Napoc. Electron. Telecommun.* **57**(3), 16–23 (2016).
119. Jansen, M. J. W. Analysis of variance designs for model output. *Comput. Phys. Commun.* **117**, 25–43 (1999).
120. Beachkofski, B. & Grandhi, R. *Improved Distributed Hypercube Sampling* (American Institute of Aeronautics and Astronautics, paper AIAA 2002-1274, 2002).
121. Jolliffe, I. T. *Principal Component Analysis* 2nd edn. (Springer, 2002).
122. Cawley, G. C. & Talbot, N. L. C. On over-fitting in model selection and subsequent selection bias in performance evaluation. *J. Mach. Learn.* **11**, 2079–2107 (2010).
123. Vinod Chandra, S. S. & Anand, H. S. Nature inspired meta heuristic algorithms for optimization problems. *Computing* **104**, 251–269 (2022).
124. Liu, J., Han, Z. & Song, W. Comparison of infill sampling criteria in kriging-based aerodynamic optimization. In *28th Int. Congress of the Aeronautical Sciences*, 1–10, Brisbane, Australia, 23–28 Sept. (2012).
125. Conn, A. R., Gould, N. I. M. & Toint, P. L. *Trust Region Methods*, MPS-SIAM Series on Optimization (2000).
126. Levy, H. & Lessman, F. *Finite Difference Equations* (Dover Publications Inc., 1992).
127. Broyden, C. G. A class of methods for solving nonlinear simultaneous equations. *Math. Comput.* **19**, 577–593 (1965).
128. Pietrenko-Dabrowska, A. & Koziel, S. Numerically efficient algorithm for compact microwave device optimization with flexible sensitivity updating scheme. *Int. J. RF Microw. CAE* **29**(7) (2019).
129. Chen, Y.-C., Chen, S.-Y. & Hsu, P. Dual-band slot dipole antenna fed by a coplanar waveguide. In *Proc. IEEE Antennas Propag. Soc. Int. Symp.*, Albuquerque, 3589–3592 (2006).
130. Pietrenko-Dabrowska, A. & Koziel, S. Simulation-driven antenna modeling by means of response features and confined domains of reduced dimensionality. *IEEE Access* **8**, 228942–228954 (2020).
131. Alsath, M. G. N. & Kanagasabai, M. Compact UWB monopole antenna for automotive communications. *IEEE Trans. Antennas Propag.* **63**(9), 4204–4208 (2015).
132. Farran, M. et al. Compact quasi-Yagi antenna with folded dipole fed by tapered integrated balun. *Electron. Lett.* **52**(10), 789–790 (2016).
133. CST Microwave Studio, ver. 2021, Dassault Systemes, France (2021).
134. Benner, P., Gugercin, S. & Willcox, K. A survey of projection-based model reduction methods for parametric dynamical systems. *SIAM Rev.* **57**(4), 483–531.
135. Pretsch, L., Arsenyev, I., Raponi, E. & Duddeck, F. Twofold adaptive design space reduction for constrained Bayesian optimization of transonic compressor blades. In *ASME Turbo Expo 2024 Turbom. Tech. Conf. and Exp.*, 1–12, London, UK, June 24–28 (2024).
136. Zhang, Z., Chen, H., Jiang, F., Yang, Y. & Cheng, Q. S. K-means-based multigroup differential evolution optimization framework for design of MIMO antenna with decoupling elements. *IEEE Antennas Wirel. Propag. Lett.* **21**(10), 1980–1984 (2022).

Acknowledgements

Author contributions

Conceptualization, S.K., A.P.; methodology, S.K. and A.P.; data generation, S.K. and A.P.; investigation, S.K. and A.P.; writing—original draft preparation, S.K. and A.P.; writing—review and editing, S.K. and A.P.; visualization, S.K. and A.P.; supervision, S.K.; project administration, S.K. and A.P.

Competing interests

The authors declare no competing interests.

Additional information

Correspondence and requests for materials should be addressed to S.K.

Reprints and permissions information is available at www.nature.com/reprints.

Publisher's note Springer Nature remains neutral with regard to jurisdictional claims in published maps and institutional affiliations.

Query Form

SREP

Journal:	**41598**	[Art. ID: **77367**]

Journal: SREP

Author: The following queries have arisen during the editing of your manuscript. Please answer queries by making the requisite corrections at the appropriate positions in the text.

Query	Details Required	Author's Response
AQ1	As References [37 and 137] are same, we have deleted the duplicate reference and renumbered accordingly. Please check and confirm.	
AQ2	References [126], [127], [128], [137] are given in list but not cited in text. Please cite in text or delete them from list.	